Western&Graduate&PostdoctoralStudies

Western University
Scholarship@Western

Electronic Thesis and Dissertation Repository

2-11-2022 1:00 PM

Connexin 43 Contributes to Phenotypic Variability of the Mouse Skull

Elizabeth Jewlal, *The University of Western Ontario*

Supervisor: Willmore, Katherine E., *The University of Western Ontario*
A thesis submitted in partial fulfillment of the requirements for the Master of Science degree in Anatomy and Cell Biology
© Elizabeth Jewlal 2022

Follow this and additional works at: https://ir.lib.uwo.ca/etd

Part of the Animal Structures Commons, Developmental Biology Commons, Musculoskeletal System Commons, and the Other Ecology and Evolutionary Biology Commons

Abstract

The purpose of this study was to determine whether connexin 43 (Cx43) contributes to craniofacial phenotypic variability. Skull shape and variation were compared within and among two heterozygous mutant mouse models (G60S/+ and I130T/+) that exhibit different levels of Cx43 channel function when compared to their wildtype counterparts (~80% and ~50% reduction in function, respectively). Results indicated mutants have significant differences in skull shape compared to wildtype littermates. Similar patterns of shape difference were found in both mutants. Increased skull shape variation and a disruption in the covariation of skull structures were observed in G60S/+ mutants only. These results show that while a 50% reduction in Cx43 function causes a shift in mean skull shape, there is a lower threshold at which Cx43 function disrupts craniofacial phenotypic robustness. This study demonstrates that Cx43 can contribute to phenotypic variability of the skull through a nonlinear relationship between Cx43 function and phenotypic outcomes.

Keywords

Summary for Lay Audience

The skull is complex in its development and function. This complexity makes it vulnerable to disruptive forces, and upwards of one third of inherited abnormalities in humans involve the skull. Abnormalities in the skull can be viewed as extreme examples of variation, and it is generally assumed that both normal and extreme variation is structured through development. If this assumption is correct, then we would expect that patterns of variation will be similar if the developmental mechanisms are similar, and that shape variation can then be used to help uncover potential areas of developmental disruption in the case of unusual development. This study tests the hypothesis that the function of a protein important for communication between cells, particularly those in bone (connexin 43), has a nonlinear relationship with how susceptible the skull is to shape change. This hypothesis was tested using mutant mice with normal and abnormal skull shapes. Two mouse models with mutations to the gene encoding for connexin 43 (Cx43) were used to test the relationship between Cx43 function and shape variation in the skull. The I130T/+ mutant mouse has a fifty percent reduction in channel function, whereas the G60S/+ mutant has an eighty percent reduction. Therefore, it was predicted that the G60S/+ mutants would have a greater difference in shape than I130T/+ but that the localization of shape differences would be similar in both mutants. Shape analyses indicated that the two mutants have significantly different skull shapes compared to non-mutant littermates. As predicted, shape changes and shape variation are more severe in G60S/+ mice than the I130T/+, but the areas and patterns of change are similar in both mutants. While the fifty percent reduction in Cx43 in I130T/+ mice was enough to change the mean shape, the range of variation (or variability) was only increased in the G60S/+ mutants, meaning that there is a nonlinear relationship between phenotype and function in the skull. This study supports the suggestion that any gene that contributes to trait development can likewise modulate trait variability, extending to genes that play important though not crucial roles in development.

Acknowledgments

Table of Contents

List of Tables

List of Figures

Chapter 1

1   Introduction

Phenotypic variation is the raw material on which natural selection acts and is therefore necessary for evolutionary change. However, excessive variation results in congenital malformations. Thus, a balance must be struck between factors that introduce and factors that constrain variation. Not all traits exhibit the same balance between variation and constraint. The skull is particularly susceptible to factors that introduce variation. Indeed, three quarters of all congenital defects involve craniofacial structures in humans (Chai & Maxson, 2006). These congenital defects can be viewed as extreme demonstrations of normal variation. The high prevalence of congenital anomalies of the skull is likely due to the skull's extremely complex development. Each bone in the adult skull forms from several ossification centers that must grow and fuse in a coordinated fashion. Furthermore, the skull is composed of bones derived from both neural crest and mesoderm cell populations that are formed through intramembranous and endochondral ossification. This developmental complexity provides great opportunity for variation to arise. However, the functional demands of the skull, such as facilitating breathing, mastication, and encasing the brain, requires that individual bones of the skull develop in concert to form a functional whole. Thus, while there are many opportunities for variation in the skull to arise, the range of observable variation is finite due to functional demands (Wagner & Altenberg, 1996). This range of possible variation describes the variability of the skull.

In this study the concept that variability is at least in part determined by embedded properties of skull development is addressed. Specifically, the study seeks to determine if nonlinearities between gene function and resultant phenotype contribute to skull variation. The remainder of this chapter outlines the historical context for the study of skull variability and provides the background and rationale for the mouse models used.

1.1   Phenotypic Variation

An organism's phenotype is composed of an observable suite of morphological traits. While many organisms exhibit similarities or trends in their appearance, no two creatures are identical. These differences are represented as phenotypic variation and can be measured and compared among different individuals or groups. Phenotypic variation arises due to a multitude of factors, including genetic variation and environmental influence. Not all traits or individuals are equally susceptible to these influences, and thus the range of variation differs depending on the robusticity or resilience of each trait and organism. This range of possible variation, or *potential* for variation within a trait, is called phenotypic variability. While phenotypic variation can be measured directly, phenotypic variability is a relational property that describes the extent of possible variation within a population in comparison with another (Wagner & Altenberg, 1996).

Phenotypic variation is the raw material upon which natural selection acts; it is necessary for the evolution of traits. However, large morphological deviations from the trait mean are usually deleterious (Hallgrímsson, Willmore, & Hall, 2002). Therefore, a balance must be struck between processes that allow and constrain variation. A consequence of leaving room for beneficial variation is that detrimental variation is also given an opportunity to occur (Willmore, Young, & Richtsmeier, 2007). These changes in variation may occur over long periods of evolutionary time, or much quicker in response to acute environmental stimuli. Recently it has been shown that several animal species are adjusting morphologically to adapt to the environmental pressures of climate change (Ryding et al., 2021). Those organisms capable of swift adaptation that does not jeopardize functional viability will be more likely to propagate and pass on genetic information. While these organisms may be able to adapt quickly to external changes, some of the phenotypic consequences may be unfavourable for long term evolutionary development.

To model these phenotypic consequences, studies of phenotypic variation and variability have often used model organisms, such as mice. These model systems allow researchers to manipulate either environmental (Breno, Bots, & Van Dongen, 2013; Gonzalez et al., 2014; Lazić et al., 2016; Waddington, 1957) or genetic (DeLaurier et al., 2014; Dun &

Fraser, 1958, 1959; Heuzé et al., 2014; Rendel, 1959) factors, such that the amount and patterning of phenotypic variation can be compared among experimental groups. The rationale for using these experimental models is that by disrupting the system through either genetic or environmental perturbations, variation that was "hidden", or buffered in the unperturbed population, will be revealed (Rutherford, 2000), providing a window into the potential for phenotypic variation. The assumption is that the variation in the perturbed and unperturbed populations is not simply random; rather it is structured by underlying developmental processes (Hallgrímsson, Willmore, & Hall, 2002).

1.2 Phenotypic Variability

1.2.1 Waddington's Epigenetic Landscape

An early visual metaphor representing how development contributes to phenotypic variation is Waddington's epigenetic landscape(Waddington, 1957) (Figure 1). In this visual metaphor, the development of a trait is represented as a ball rolling down a hill and the distance between the top and the bottom of the hill represents developmental time. The potential developmental trajectories of a trait, as informed by the underlying genetic makeup, are represented as a series of grooves within the hill that all lead to a specific phenotypic outcome. In this visualization of the metaphor (Figure 1), some of these outcomes are phenotypically normal for a population, here represented by the bins defined as -1 to +1 standard deviations. Other trajectories lead to abnormal morphology, represented by the bins defined as +/- 2 and 3 standard deviations. The path the ball takes down the hill is dependent on the depth of the grooves as well as potential genetic and environmental perturbations. Genetic and environmental perturbations act to push the ball horizontally, or reduce the depth of the grooves, potentially knocking the ball from one groove or trajectory to another. Trajectories represented as deep grooves are more robust to such perturbations, and allow the ball to maintain its original path, whereas shallow grooves allow for more flexibility, enabling the ball to be more easily displaced to adjacent trajectories. This "landscape" differs among individuals, with some individuals' development represented by deep grooves indicating high developmental fidelity or resilience and others represented by shallow grooves leaving their development more vulnerable to genetic and environmental insults. Thus, the possible distribution of the

balls describes the phenotypic variability. The larger the range of outcomes, the greater the variability.
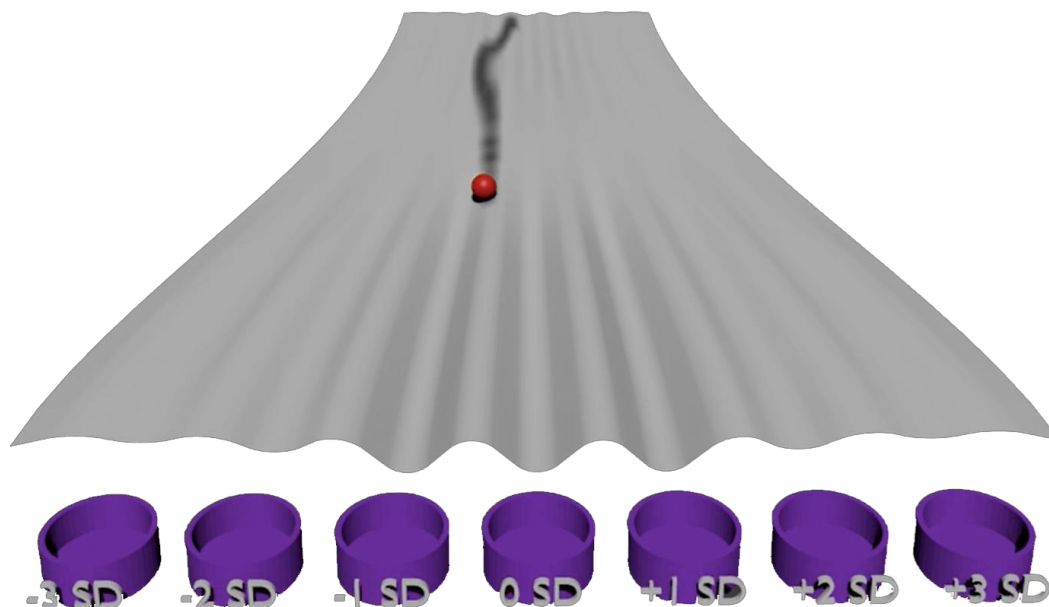
Figure 1 Illustration of Waddington's epigenetic landscape

The concept of the epigenetic landscape is here represented by the grey ramp. The ball rolling down the hill signifies the developmental processes over time that produce the resultant phenotype. The purple baskets represent the phenotype in relation to standard deviations (SD) from the mean trajectory.

Phenotypic variability is often described and studied through three related concepts: canalization, developmental stability, and morphological integration (Hallgrímsson, Willmore, & Hall, 2002). These concepts or components of variability are linked in that they describe the relative buffering of development against genetic and environmental perturbations. However, each of these components captures different aspects of phenotypic variation and subsequent variability (Willmore et al., 2007). Each of these concepts is defined and described below.

1.2.2   Canalization

Canalization refers to the suppression of phenotypic variation among individuals, and Waddington proposed that canalization occurs through development itself (Waddington, 1942; Waddington, 1957). While canalization provides phenotypic robustness among individuals, it enables variation at the genetic, cellular, and tissue levels, thus maintaining the evolutionary potential of complex traits (Wagner & Altenberg, 1996). The early studies of canalization used assimilation experiments to look at *Drosophila* phenotype when treated with ether to induce a targeted phenotype. Waddington found that after several generations, the induced phenotype began to arise without an external stimulus (Waddington, 1953; Scharloo, 1991). Subsequent studies demonstrated that genetic or environmental insults can uncover genetic variation that is normally "hidden" by buffering properties of development (Rutherford & Lindquist, 1998; Wilkins, 2002).

1.2.3   Developmental Stability

Where canalization homes in on the suppression of among-individual variation, developmental stability focuses on the regulation of within-individual variation (Clarke, 1998). This variation arises due to the fallibility of the developmental processes themselves rather than from the effects of external perturbations (Hallgrímsson, Willmore, & Hall, 2002; Van Valen, 1962). Developmental stability impacts the evolutionary potential for those traits responsible for the most basic functions, such as translation, transcription, and protein folding (Klingenberg, Barluenga, & Meyer, 2002). For organisms that are more developmentally stable, the variability within an individual would be low. As the system experiences an increase in noise, there is an assumption that an increase in within-individual variation will follow. This assumption does not always hold true, and this suggests the existence of a threshold that must be crossed to see a significant increase in variation (Klingenberg, Barluenga, & Meyer, 2002).

1.2.4   Morphological Integration

The final piece that contributes to phenotypic variability is morphological integration. Morphological integration describes the interrelation that exists between one or more traits (Olson & Miller, 1958). For example, phenotypic traits that are closely linked

through function, location, or development often exhibit a certain amount of morphological integration. An example of this could be the morphology of the brain and chondrocranium, which are closely linked through development. Integration can be observed at the individual, genetic, and evolutionary level (Cheverud, 1996). Integration between traits increases the likelihood of certain phenotypes being perpetuated through natural selection. Those traits that are tightly integrated are referred to as modules. Traits within a module are more likely to evolve independently from traits from other modules (Klingenberg, 2008). Thus, the study of integration and modularity allows for insight on how variation is structured and can uncover meaning in those patterns of variation that are observed.

1.3   Measures of Phenotypic Variation

1.3.1   Geometric Morphometrics

A common method of measuring phenotypic variation is geometric morphometrics, or the statistical analysis of shape and size using 2D or 3D landmark data. Landmarks are selected based on their biological significance, repeatability, and their coverage of the trait(s) of interest (Zelditch, Swiderski, & Fink, 2004). Biologically significant landmarks are selected to be repeatable across individuals and reduce the amount of noise created by intra-rater error. Individuals are landmarked twice, and the mean is taken to determine the final dataset. To interpret this complex shape data, it is necessary to fit each individual into the same shape space. This fit is accomplished using Procrustes superimposition, a threefold technique that scales, rotates and superimposes the data, giving each individual a new set of Procrustes landmark coordinates that are used for subsequent statistical analyses (Zelditch, Swiderski, & Fink, 2004). Several techniques exist for the study and assessment of these data, with the current field standard being the analysis of data with several open-sourced suites in the R statistical computing software. These suites allow for a consistency in data analysis and interpretation across the field and due to the open-source nature, are consistently updated.

1.3.2   Among-Individual Variation

Canalization is most commonly assessed through the measurement of among-individual variation, with greater canalization represented by low variation. The amount of trait variation within one or more experimental groups compared with a control group indicates how well canalized the trait is against genetic and environmental insults. Shape variation can be measured from multivariate landmark data using a non-parametric MANOVA on Procrustes distances. Multivariate analyses allow for the 3D landmark shape data to retain their spatial relationship information when multiple landmark coordinates must be used to represent individual shape (Adams & Collyer, 2018).

Shape variation can also be visualized through several means, including principal components analysis (PCA) and trajectory analysis. PCA looks at the axes responsible for the most variation in a population and assigns a score to each individual for each principal component (PC). The majority of variation is captured within the first few PCs, greatly simplifying the data, which can then be visualized on a scatterplot, with each point representing an individual. The grouping of individuals offers a method of mean shape comparison within and among groups of interest, with overlap of PC scores indicating similar shape and distinct clusters indicating differences in mean shape. Variation in shape is depicted by the spread of PC scores along the axes. The greater the spread of points, the greater the variation among individuals, which implies reduced canalization. Another means of measuring and visualizing canalization is through trajectory analysis. This method uses principal components to visualize the magnitude and direction of shape change between two or more groups.

1.3.3   Fluctuating Asymmetry

The standard measure of developmental stability is within-individual variation as assessed by fluctuating asymmetry (FA). FA is the measurable expression of left-right asymmetry of bilaterally symmetrical morphological structures (Klingenberg, 2003). When the internal environment of an organism experiences a critical amount of noise, this can be visualized through an increase of FA. FA can be visualized using some of the same techniques as among-individual shape variation. Principal components analysis can

show the within-group range of FA as well as allow for among-group comparisons (Klingenberg, Barluenga, & Meyer, 2002).

1.3.4   Phenotypic Covariation

To measure morphological integration, covariation between traits is calculated. Covariation can be explored using an *a posteriori* approach to determine which traits may share enough similarities to form distinct groups or modules of interest. Covariation can also be measured using Procrustes superimposed datasets whose landmarks have been subdivided into *a priori* modules (Olson & Miller, 1958; Cardini, 2019). Covariation between those modules can be measured and visualized using a two-block partial least squares (PLS) analysis. The method used in this study looks at *a priori* modules based on the developmental subregions of the skull (mesoderm- and neural crest-derived tissues, and endochondral and intramembranous bones). This allows us to assess if predetermined developmental factors are strongly integrated, and if this integration changes following a genetic perturbation.

1.4   Mechanisms that Modulate Phenotypic Variation

The mechanisms that modulate phenotypic variation are not mutually exclusive, and it is likely that to truly understand robusticity of traits, an understanding of multiple mechanisms is required (Hallgrímsson, et al., 2019). This section acts to highlight some of the mechanisms that have been previously investigated, and how they have been found to modulate phenotypic variation.

One specific mechanism that has been shown to modulate variation is protective function of heat shock proteins (HSPs). HSPs are a group of proteins that function in cells when they are exposed to stress conditions. Studies have shown that a decrease in HSP levels can significantly impact the evolutionary potential of multiple traits in *Drosophila* (Rutherford & Lindquist, 1998; Sørensen, Kristensen, & Loeschcke, 2003). Rutherford & Lindquist observed that Hsp90 levels in *Drosophila* impact evolutionary change by helping to buffer a multitude of developmental pathways. When Hsp90 function was reduced, there was an increase of phenotypic variation of several traits (Rutherford & Lindquist, 1998). Variation can see both a rise and fall after HSP recruitment during

stress times. While HSP recruitment in response to stress may initially prevent an increase in phenotypic variation, upon hitting a threshold HSPs are no longer available to mitigate these changes. Indeed, it may prove that deletion or failure of a gene has a less dramatic impact on variation than the reduction in chaperone function, due to the vast network of processes that HSPs buffer (Rutherford, 2003).

A fundamental biological mechanism that has been shown to modulate phenotypic variation is the role of microRNAs (miRNAs). miRNAs act to repress gene expression and regulate transcription. Similar to HSPs, miRNAs can have a profound effect on multiple developmental processes. miRNAs have been shown to act as buffers against variation (Ebert & Sharp, 2012). It has been shown that miRNA experiences a threshold effect, which helps to suppress different genes, and thus phenotypic outcomes. This indicates that miRNA may act in concert with other developmental mechanisms to help stabilize phenotypic variability (Ebert & Sharp, 2012).

It is important for a certain amount of variability to exist among traits. This variability must allow for positive change, while maintaining stability. This relationship has been posited to be nonlinear in nature. Nonlinearity is then the observance of a threshold at which traits exhibit an influx of variation that is not necessarily proportional to the amount of external perturbation. This nonlinearity is thought to be modulated by developmental processes. Ramler et al. found that the effect of temperature on phenotypic variation exhibited a nonlinear relationship when observing how a wide range of temperatures impacted the phenotype of a threespine stickleback fish (Ramler et al., 2014). By including a wide range of temperatures, this study was able to model the threshold at which phenotypic variability increased. In another study, Green et al. demonstrated a nonlinear relationship between *Fgf8* expression and craniofacial development in mice, wherein mouse facial development was robust to a 60% reduction in *Fgf8* levels, whereas beyond this threshold, small changes in gene expression resulted in large phenotypic effects (Green et al. 2017). Through this nonlinear relationship, a large amount of genetic variation can be tolerated without phenotypic consequence. While there is compelling evidence that the effects of genetic and environmental insults can be buffered by specific, dedicated developmental mechanisms for complex traits such

as skull shape, phenotypic robustness may arise more commonly through general developmental mechanisms such as nonlinearities (Hallgrìmsson et al. 2019). In contrast to previous studies of nonlinearities, this study seeks to determine if a gene that is important but not crucial to skull development contributes to phenotypic variability.

1.5   Craniofacial Development

To further the aim of studying how developmental mechanisms, like nonlinearities, impact phenotype it is helpful to focus on a specific region that is measurable, developmentally complex, and prone to a wide range of phenotypic variation in both normal and abnormal development. The skull offers such a complex structure, in that it requires several mechanisms working in concert to allow for proper development, which allows for a wide range of possible phenotypes. These abnormal phenotypes can occur during early development, such as neurocristopathies (Bolande, 1997), or later in life. These post-natal morphologies can arise due to mechanical injuries like temporomandibular disorder (Bavia, Vilanova, & Garcia, 2016), or diseases that impact bone remodeling (Feng & McDonald, 2011).

At the cellular level, development of the skull begins with two cell lineages, the neural crest and mesoderm. A specific subset of neural crest cells, cranial neural crest cells, undergo a series of processes including induction, epithelial-to-mesenchymal transition, migration, proliferation, and differentiation to form many of the cell types which are responsible for the creation of the facial skeleton, and part of the cranial vault (Santagati & Rijli, 2003; Chai & Maxson, 2006). In contrast, the cranial base and posterior portion of the cranial vault are formed from cells of somatic mesoderm origin (Vyas, Nandkishore, & Sambasivan, 2020). Adding to the complexity, both cell types can contribute to skull formation through two different types of ossification.

The skull ossifies through endochondral and intramembranous ossification. The flat bones of the calvaria and facial bones form through intramembranous ossification, a process in which sheets of bone develop through the proliferation of mesenchymal stem cells directly into osteoprogenitor cells. The cranial base and ossicles form through endochondral ossification, a process more commonly associated with long bone

development. Endochondral ossification is a process in which a cartilaginous model is used as a template for bone development (Marieb, Mallatt, & Wilheld, 2013). Both modes of ossification are found in cranial neural crest- and mesoderm-derived tissues, meaning there is an overlap producing four unique regions of interest - endochondral and intramembranous neural crest-derived bone, and endochondral and intramembranous mesoderm-derived bone (D'Souza, Ruest, Hinton, & Svoboda, 2010). This overlap allows for studies to examine the dynamic interplay between different developmental processes present in each region, and to determine if certain regions are more or less buffered against perturbations based on their phenotypic variation.

1.6   Connexin 43 (Cx43)

1.6.1   Connexins

The complex development of the skull, and all bone, relies on intercellular communication. One of the families of proteins that facilitate intercellular communication is connexins. Connexins are intramembranous proteins comprised of four transmembrane domains, two extracellular loops, one intracellular loop as well as an n- and c- terminus (Figure 2) (Laird, 2014). These proteins oligomerize into hexameric structures referred to as hemi-channels or connexons (McLachlan, et al., 2008). Connexons may function as hemichannels connecting the intercellular matrix with the extracellular environment, or they can bind with a connexon on an adjacent cell to form gap junctions (McLachlan, et al., 2008). Gap junctions are intercellular channels, which allow for the transfer of small molecules and secondary messengers less than 1kDa in size between cells, facilitating intercellular communication (Laird, 2014).

Mutations in the genes encoding for connexin proteins result in a wide array of human diseases due to the disruption of normal intercellular communication. These include syndromic and non-syndromic hearing loss (Cx26, Cx30, Cx31, Cx43), skin disease (Cx26, Cx30, Cx30.3, Cx31, Cx43), peripheral neuropathy (Cx32), atrial fibrillation (Cx40), cataracts (Cx46, Cx50), and bone dysplasia (Cx43) (Laird et al. 2017; Srinivas et al. 2018).

1.6.2   Connexin 43 in Bone

Due to its important role in osteogenesis, the protein of focus for this study is connexin 43 (Cx43). Of the 21 connexins expressed in humans, Cx43 is the most ubiquitously expressed and is also present in mice (Flenniken, et al., 2005). In terms of skeletal development, Cx43 is found in osteoprogenitor cells, osteoblasts, osteocytes, and osteoclasts (Stains & Civitelli, 2005). Cx43 gap junction channels allow the intercellular passage of secondary messengers such as ATP, calcium ions, and inositol polyphosphates that are thought to initiate signaling cascades important in bone development and homeostasis (Goodenough, Goliger, & Paul, 1996). Cx43 hemichannels are also thought to be important in bone homeostasis (Riquelme, Cardenas, Xu, & Jiang, 2020). Indeed, Cx43 function has been shown to play a role in osteoblast differentiation (Lecanda, et al., 2000; Chung, et al., 2006; Dobrowolski, et al., 2007; McLachlan, et al., 2008; Watkins, et al., 2011; Jarvis, et al., 2020), osteocyte mechanosensation in relation to bone remodelling, (Alford, Jacobs, & Donahue, 2003; Jiang, Siller-Jackson, & Burra, 2007; Taylor, et al., 2007; Grimston, Watkins, Stains, & Civitelli, 2013; Plotkin, Speacht, & Donahue, 2015) and osteoclast formation and activation (Ilvesaro, Tavi, & Tuukkanen, 2001; Ransjö, Sahli, & Lie, 2003).

Dysregulation of Cx43 results in a variety of functional consequences such as increased osteoclastogenesis, osteocyte apoptosis, and impaired osteoblast differentiation (Bivi, et al., 2012; Lecanda, et al., 2000). Disrupted Cx43 function can impair the normal homeostasis of both endochondral and intramembranous bone and leads to phenotypic changes, such as a decrease of cortical bone thickness and overall decrease in bone mineral density (Laird et al., 2017; Zappitelli & Aubin, 2014).

1.6.3   Mutations of Connexin 43

Cx43 is encoded by the gene *GJA1,* and there are currently more than eighty known mutations of the gene (Laird 2014). The majority of these mutations are autosomal-dominant missense mutations and are linked with the rare human condition, oculodentodigital dysplasia (ODDD) (Meyer-Schwickerath, Gruterich, & Weyers, 1957; Laird, 2014). ODDD is predominantly characterized by microphthalmia, syndactyly,

skull anomalies, cardiac defects, and enamel hypoplasia. ODDD provides a lucrative model for the study of craniofacial variation, due to the wide range in craniofacial phenotypes that are associated with ODDD. These include underdeveloped nasal bones, overgrowth of nasal cartilage, cleft palate, cleft lip, hypotelorism, small chin, and malar hypoplasia (Paznekas, et al., 2009). It is useful as a model for the study of variation, due to the high intra- and inter-familial variation in phenotypic presentation (Paznekas, et al., 2003; Paznekas, et al., 2009). While this variable phenotypic expression presents challenges in understanding the mechanisms that underlie ODDD and the role of Cx43 in bone and skull development, it also offers an opportunity to determine whether an important, though not critical, gene in skull development, such as *GJA1*, can modulate phenotypic variation.

1.7   Connexin 43 Mouse Models

Several genetically modified mouse models targeting the *Gja1* gene encoding Cx43 have been developed. Of these, three are models of ODDD, and include two models of disease-linked mutations found in humans (I130T & G138R) (Kalcheva et al., 2007; Dobrowolski et al., 2008) and one mutation, not found in humans, which resulted from an ENU-mutagenic screening (G60S) (Flenniken et al. 2005).

1.7.1   I130T/+ Mutant Mouse

The first mouse model used in this study (I130T/+) is heterozygous for an autosomal-dominant mutation found in humans with ODDD. It results from the substitution of isoleucine for threonine at the 130th residue in the intracellular loop of the Cx43 protein (Figure 2). Animals with homozygous expression of the I130T mutation are not viable due to defects in the pulmonary outflow tract, necessitating the use of heterozygotes for post-natal studies (Kalcheva et al., 2007). This mutation was found to cause a 50% decrease in channel conductance (Laird, 2014). The resulting murine phenotype was found to be similar to that of humans with ODDD (Paznekas, et al., 2009; Jarvis, et al., 2020).

Previous studies in our lab have used the I130T/+ mouse model to determine that there is a significant difference in skull shape and size between adult I130T/+ and wildtype mice

as newborn pups and adults, and that the ODDD phenotype arises between E17.5 and birth in these mice (Jarvis, et al., 2020). The phenotype was found to get worse over time with the greatest differences in morphology observed in bones of the face (Jarvis, et al., 2020).
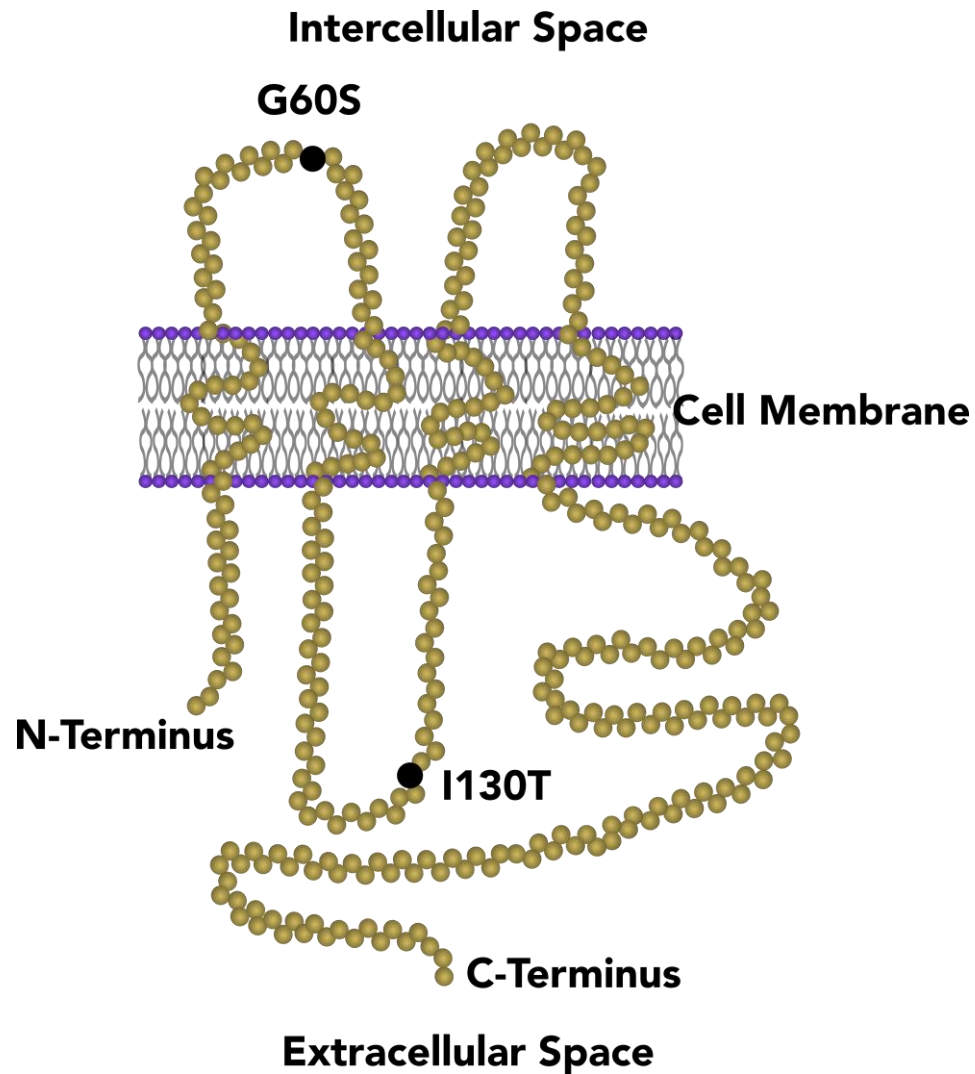
Figure 2 Connexin 43 protein

Schematic of the protein connexin 43 highlighting the locations of the mutations found in our two mouse models of ODDD indicated by black dots. The G60S mutation is located on the first extracellular loop and the I130T mutation is located on the intracellular loop.

1.7.2   G60S/+ Mutant Mouse

The second model used in this study (G60S/+) is heterozygous for the missense point mutation between glycine and serine at the 60th residue on the first extracellular loop (Figure 2). The consequences of this dominant-negative mutation are far more severe than those of the I130T/+ mutation, reducing Cx43 channel function to 15-20% along with a reduction of Cx43 expression. It has yet to be discovered in human patients with ODDD and was discovered through N-ethyl-N-nitrosourea (ENU) mutagenesis screening. Mice with the G60S/+ mutation were found to have an ODDD-like phenotype, including syndactyly, underdeveloped incisors, eye malformations, osteopenia, and differences in skull morphology (Flenniken et al., 2005). Additionally, previous work in our lab has demonstrated that mandibular morphology in newborn G60S/+ and I130T/+ mice is significantly different from their wildtype littermates (Moore, et al., 2020).

1.8   Rationale

It has long been posited that phenotypic variability is modulated by developmental processes, and Waddington suggested that embedded properties of development may play a role in regulating variation (Waddington, 1957). Recent studies have demonstrated that emergent properties of development such as a nonlinearity between gene dosage and phenotypic outcome can explain variability in skull phenotype (Green, et al., 2017). However, these studies have focused on the role of genes of critical importance to skull development (eg. *Shh*, *Fgf*, *Wnt*) (Young, Chong, Hu, Hallgrímsson, & Marcucio, 2010; Dash & Trainor, 2020), and it is yet to be determined if genes encoding proteins that play active, though not crucial, roles in skull development, can likewise modulate phenotypic variation. The aim of this study is to determine if Cx43 modulates variability of the skull. Cx43 has been shown to play an active role in bone development and homeostasis (Stains & Civitelli, 2005). Disruptions to Cx43 function through mutation result in the human disease ODDD, which presents with a distinct craniofacial phenotype (Meyer-Schwickerath, Gruterich, & Weyers, 1957). Two heterozygous mouse models, G60S/+ and I130T/+, show a distinct ODDD-like phenotype, which results from a common disruption to normal Cx43 function (Flenniken, et al., 2005; Kalcheva, et al., 2007). The difference in severity of phenotype, with G60S/+ mice seemingly more strongly impacted

than I130T/+, provides an ideal model for the study of how disruption to a non-crucial gene (*Gja1*) impacts phenotypic variation and variability, and if this impact is linear or nonlinear in nature. Determining the linearity or nonlinearity in a specific developmental process can show which traits are buffered against external influence (Jewlal et al., 2021).

1.9   Hypothesis

Given the role of Cx43 in non-pathological skull development, I hypothesize that it also plays a role in modulating phenotypic variability of the skull through developmental nonlinearities between Cx43 channel function and resultant phenotype.

1.10   Objectives and Predictions

If the mechanisms that regulate phenotypic variability are embedded processes of development, then I predict that not only crucial genes, such as Wnts and Fgfs, but also other genes that play an important though not critical role in trait development, will be able to modulate variability. This prediction was tested by comparing skull phenotypes among mice with different levels of Cx43 function. Specifically, we used 3D landmarks from micro-computed tomography (µCT) reconstructions of newborn and 3-month G60S/+, I130T/+ mice, and their wildtype littermates to measure and compare skull size, mean shape, shape variance, shape asymmetry, and covariation among genotypes using geometric morphometrics.

1.10.1   Objective 1

The first objective of this study is to characterize and compare skull shape and size among G60S/+, I130T/+ mutant mice, and their wildtype littermates at birth and 3 months to assess the linearity between mean phenotypic outcomes and the degree of Cx43 channel function.

1.10.2   Objective 1 Predictions

1.10.2.1

Given the active role of Cx43 in bone development and remodeling, I predict that the larger deficit in Cx43 channel function in G60S/+ mice will result in greater changes in

skull shape and size than those observed in the I130T/+ mutant mice and that these phenotypic changes will scale with Cx43 function in a nonlinear fashion.

1.10.2.2

Given the common developmental disruption, I predict that the same skull traits will be targeted in G60S/+ and I130T/+ mice as observed by similarly localized differences in mean shape and size between mutants and wildtype littermates.

1.10.3   Objective 2

To measure and compare the amount and structure of phenotypic variation of the skull among G60S/+ and I130T/+ mutant mice, and their wildtype littermates at birth and 3 months. The degree of skull variation and the structure of this variation is determined through measures of among-individual variation, within-individual variation (FA), and covariation among genotypes.

1.10.4   Objective 2 Predictions

1.10.4.1

I predict that both mutant models will have increased among- and within-individual variation compared with their wildtype littermates and that G60S/+ mice will display a nonlinear increase in skull variation in comparison with I130T/+ mice.

1.10.4.2

As both mutant mouse models disrupt Cx43 and alter similar processes in bone development, I predict that the patterns of variation and covariation will be similarly localized.

Chapter 2

2 Materials and Methods

2.1 Mouse Models

Skull size, shape, shape variation, FA, and covariation were compared among G60S/+ mice and their wildtype littermates and I130T/+ mice and their wildtype littermates at post-natal day 0 (P0) and 3 months. A sample size of 30 mice/genotype/age with an equal sex distribution was used for all analyses. G60S/+ mice were created from ENU mutagenized C57BL/6 male mice and bred on a C3H/HeJ background (Flenniken, et al., 2005), and I130T/+ mice were created on a mixed C57BL/6 and CD1 background and subsequently bred on a C57BL/6 background (Kalcheva, et al., 2007). Prior to sacrifice, all mice were visually sexed, and genotyped using tail samples (Moore, et al., 2020; Abitbol, et al., 2018). Mice were housed in standard cages and maintained on a 12hr light/dark cycle, with a diet of standard mouse chow (2018 Teklad Global 18% Protein Diet, Harlan Laboratories, Indianapolis, IN, USA). G60S/+ and their wildtype littermates were supplemented with powdered food due to significant enamel hypoplasia in mutants (2920X Teklad global soy protein-free extruded rodent diet; Harlan Laboratories, Indianapolis, IN, USA) (Flenniken, et al., 2005). The study was conducted in accordance with the policies and guidelines of the Canadian Council on Animal Care and approved by the Animal Care Committee of the University of Western Ontario.

2.2 Imaging of Mouse Skulls

Prior to imaging, mouse heads were placed in phosphate-buffered saline and skin was dissected. Heads were then fixed in 4% paraformaldehyde for 12-24 hours, mounted on foam and embedded in 1% agarose in 50mL Falcon tubes to prevent movement during scanning (Jarvis, et al., 2020). P0 mice were imaged using high-resolution μCT (20 μm isotropic voxel size) using a GE Locus RS-9 x-ray μCT scanner (GE Healthcare, USA) housed in the Preclinical Imaging Facility at Robarts Research Institute (UWO, London, ON, CAN). 900 views per gantry rotation were acquired over a 360-degree rotation. Projections lasted for 4500 ms with potential measured at 80 kVp and tube current measured at 450 μA. Three-month mouse skulls were scanned at 20 μm isotropic voxel

size using a Nikon XTH 225 ST cone-beam µCT scanner (Nikon Metrology Inc., UK) housed at Sustainable Archaeology (UWO, London, ON, CAN). 3141 projections were acquired over a 360-degree rotation. Projections lasted 1000 ms with potential measured at 88 kVp with a tube current of 95 µA. A phantom consisting of air, water, and a cortical bone mimicking epoxy with a bone mineral equivalent of 1100 mg cm^{-3} (SB3, Gamex, USA) was used in each scan for consistency of Hounsfield Unit calibration and material registration (Beaucage, et al., 2014; Caskenette , et al., 2016).

2.3   3D Landmark Collection

3D landmarks were chosen based on their ability to capture the most complete representation of the skull geometry and homology among age groups as described previously (Abitbol, et al., 2019; Jarvis, et al., 2020). Landmark data were collected for each mouse skull using Checkpoint software (Stratovan Corporation, Davis, California, USA) from volumetric reconstructions of µCT data at consistent thresholds in MicroView (Parallax Innovations, Ilderton, ON, Canada). To assess landmark repeatability and enable measurement and comparison of FA, the skulls were landmarked twice, ensuring that points could be repeated within 0.05 mm of error (Frelat, et al., 2012). The average of the two trials was used in all subsequent analyses except for comparisons of FA.

2.3.1   Procrustes Superimposition

Prior to analysis, landmark data undergo Procrustes superimposition, a threefold process in which the 3D landmark coordinates undergo translation, scaling, and rotation. This process acts to fit all the coordinates within the same shape space, creating the Procrustes Average Shape. Points are reclassified with Procrustes coordinates, which are used in subsequent analyses.

Data underwent Procrustes superimposition using the *geomorph* package in R (Adams, et al., 2016; R Foundation for Statistical Computing, Vienna, Austria, 2017). To enable localized shape and size comparisons among genotypes, biologically relevant subsets of landmarks were created based on tissue origin (neural crest-derived and mesoderm-derived) and mode of ossification (intramembranous and endochondral) (Figure 3A).

Separate superimpositions were conducted for the whole skull and each regional subset. To account for differences in genetic background, Procrustes superimposed data were centered for each genotype on the grand mean (Green, et al., 2017). Thus, all comparisons except the trajectory comparisons used pooled within-genotype analyses.

2.4   Skull Size Comparison

Skull size and size of regional skull subsets were measured and compared using centroid size, a non-unitary measure determined by summing the squared distance between each landmark in a configuration and the centre point. To account for gross size differences between mutants and wildtype mice and potential sexual dimorphism, centroid size was regressed on body weight and these scaled size measures were used in comparisons. Statistical comparisons of scaled skull centroid size among genotypes were performed using a two-way ANOVA with genotype and sex as main effects. Subsequent pairwise comparisons between treatment groups were conducted using the glht function from the *multcomp* package in R (Hothorn, Bretz, & Westfall, 2008; R Foundation for Statistical Computing, Vienna, Austria, 2017). Similarly, comparisons of scaled centroid size were performed on each regional subset of landmarks to determine potential localized size differences.

2.5   Skull Shape Comparison

Skull shape was assessed to determine if reduced Cx43 function results in similar phenotypic differences. Shape differences were compared among genotypes via a two-way MANOVA with genotype and sex as main effects using the procD.lm function in the R package *geomorph* (Adams, et al., 2016). This function includes resampling using 10,000 iterations to create a probability distribution from which significance ($\alpha=0.05$) can be determined (Collyer, Sekora, & Adams, 2015). To illustrate localized shape differences between mutants and their wildtype littermates and between the G60S/+ and I130T/+ mutants, we constructed heat morphs using the *rgl* package in R (R Foundation for Statistical Computing, Vienna, Austria, 2017). To visualize shape differences between genotypes, heat morphs were created wherein the degree of shape differences was demonstrated by colour differences using R (R Foundation for Statistical Computing,

Vienna, Austria, 2017). To allow visualization of the range of phenotypic differences among mouse groups, these comparisons were made between mice that fell at the extreme ends of PC1 using the symmetric component of the superimposed data.

2.5.1   Trajectory Analysis

Trajectory analyses were used to further compare the nature of skull shape differences exhibited by G60S/+ mice and their wildtype littermates and I130T/+ mutants and their wildtype littermates. Specifically, trajectory analyses enabled us to compare the magnitude and direction of shape differences between each mutant and their respective wildtype littermates. These analyses were conducted using the trajectory.analysis function in *geomorph* on data that did not undergo centering on the grand mean (Adams & Collyer, 2009).

2.6   Comparison of Skull Shape Variation

To determine how Cx43 function affects phenotypic variation of the skull, both skull shape variation and FA were measured and compared among genotypes. Skull shape variation was compared using the symmetric component of the centred Procrustes data using the morphol.disparity function in the R package *geomorph* (Adams, et al., 2016). This function estimates shape variation based on Procrustes distances using a series of 10,000 iterations and then conducts pairwise comparisons. Comparisons of skull shape variance were conducted for the whole skull and each regional subset. Skull shape variation among genotypes was visualized using principal components analyses (PCA), which depict the direction and magnitude of shape variation within and among the genotypes. Principal component scores of each mouse for the first two principal components (PC1 and PC2) are shown as a scatterplot; a greater spread of PC scores indicates greater shape variation.

2.6.1   Fluctuating Asymmetry

Fluctuating asymmetry was measured and compared among genotypes to determine the effects of Cx43 channel function on skull variation at a highly localized phenotypic scale. To measure and compare FA within genotypes, the bilat.symmetry function in the R

package *geomorph* was used and the FA component was extracted from the function's output (Klingenberg, et al., 2002; Adams, et al., 2016). The FA component of shape was illustrated using heat morphs created using the *rgl* package in R (R Foundation for Statistical Computing, Vienna, Austria, 2017). The effects of Cx43 function on FA were determined using the morphol.disparity function in *geomorph* (Adams, et al., 2016). As with among-individual variation analyses, a series of pairwise comparisons between genotypes was performed using the morphol.disparity function and these comparisons were conducted for whole skull and regional subset data. Visualization of the degree of FA within each genotype was accomplished using PCA on the FA component of the data. Individual scores for PC1 and PC2 were graphed in a scatterplot, and as with our PC graphs of skull shape variation, the greater the spread of points for a genotype, the greater the FA. Additionally, to visualize the regional differences in FA between genotypes, heat morphs were created as described for shape comparisons only using the FA component of the superimposed data.

2.7   Comparison of Covariation within the Skull

Covariation between skull traits formed through intramembranous and endochondral ossification and between structures derived from neural crest and mesoderm was measured and compared among genotypes using group mean centred two-block PLS analyses (Rohlf & Corti, 2000; Adams & Collyer, 2016). These tests were compared for both P0 and 3-month mice using the integration.test function in the R package *geomorph* (Adams, et al., 2016; Adams & Collyer, 2016). For each two-block analysis, the maximal correlation between blocks or regional subsets (rPLS) and the strength of covariation were statistically compared among genotypes using the effect size (z score) of covariation (Adams & Collyer, 2016). Covariation between regional subsets of the skull for each genotype was illustrated using scatterplots of individual scores for the first PLS axis (PLS1) for each block or subset.

Chapter 3

3   Results

To determine the effects of Cx43 function on phenotypic variability of the skull, we compared skull size, shape, shape variation, and covariation between G60S/+ mice and their wildtype littermates (WT-G60S), between I130T/+ mutants and their wildtype littermates (WT-I130T), and between both mutants at P0 and 3 months. Because the different mutant mice are on separate genetic backgrounds (Flenniken, et al., 2005; Kalcheva, et al., 2007), superimposed landmark data were centered for each genotype on the grand mean to remove the effects of mouse strain and allow comparison between mutant mice (Green, et al., 2017).

3.1   At age 3-months, mutant skulls are smaller than wildtype with greatest size reduction observed in the G60S/+ strain

To determine the effects of reduced Cx43 function on skull size, centroid size was calculated from landmark data and scaled for body mass. To enable measurement and comparison of localized effects associated with each mutation, we created subsets of landmarks based on tissue origin (neural crest-derived and mesoderm-derived) and mode of ossification (intramembranous and endochondral) (Figure 3A). Scaled centroid size was then calculated for and compared among genotypes for the whole skull as well as each regional subset. At P0, differences in skull size among genotypes were only found in regions of the skull developed through intramembranous ossification, and regions of neural crest origin (Figure 3B, C). For intramembranously ossified bones, both mutants were significantly smaller than their wildtype littermates. Only I130T/+ mutants had smaller neural crest-derived structures compared to their wildtype littermates. By 3 months, overall skull size and size of regional subsets of the skull were significantly smaller in both mutant mice compared to their wildtype littermates (Figure 3B, D). G60S/+ mice had a more extreme reduction in skull size compared to their wildtype littermates and were significantly smaller than I130T/+ mutants for all regions of the skull except for the mesoderm-derived subset.

Comparisons of skull centroid size included sex as a factor to determine if there were sex effects for skull size. Sex effects were not significant at P0, with the exception that female G60S/+ mice were significantly larger than male G60S/+ mice for the neural crest-derived region (p = 0.036). At 3 months, however, females had significantly larger skulls than males for all genotypes and regions, except for comparisons between male and female G60S/+ mice for the intramembranous (p = 0.06) and endochondral (p = 0.208) regional subsets. Importantly, while strong sex effects were found at 3 months, no significant genotype-by-sex interactions were detected, indicating that this dimorphism was not affected by either mutation.
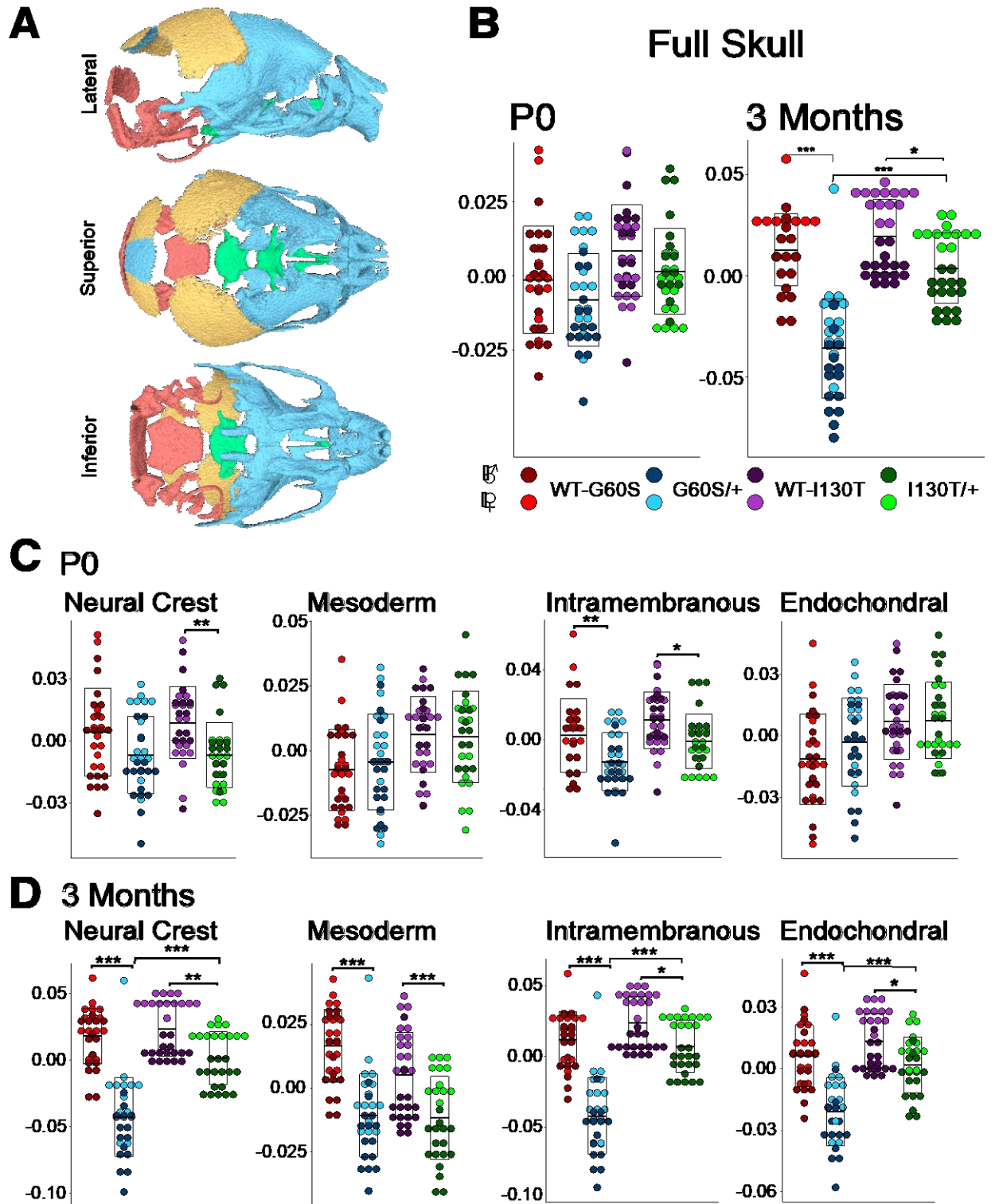
Figure 3 Mutant mouse skulls are significantly smaller than their wildtype littermates at 3 months.

A: Coloured P0 mouse skull illustrating different subregions. Red represents bone of mesoderm origin and endochondral ossification. Yellow represents bone of mesoderm origin and intramembranous ossification. Blue represents bone of neural crest origin and intramembranous ossification. Green represents bone of neural crest origin and endochondral ossification. Relative skull size was measured as centroid size regressed on body mass. B: Comparisons of relative whole skull size among genotypes at P0 and 3 months. C: Comparison of size of regional subsets of the skull among genotypes at P0. D: Comparison of size of regional subsets of the skull among genotypes at 3 months. *P <.05, **P <.01, ***P <.001.

Table 1. Skull Shape Comparisons Among Genotypes at P0 and 3 Months

P0	Whole Skull		Neural Crest		Mesoderm		Intramembranous		Endochondral	
	Gen	Sex	Gen	Sex	Gen	Sex	Gen	Sex	Gen	Sex
WT-G60S : WT-I130T	**0.012**	0.483	0.449	0.639	**0.002**	0.355	**0.010**	0.441	0.179	0.775
WT-G60S : G60S/+	**0.0001**	0.103	**0.0002**	0.071	**0.0001**	0.189	**0.0001**	0.116	**0.0001**	0.061
WT-I130T : I130T/+	**0.002**	**0.0002**	**0.0002**	**0.0001**	**0.021**	**0.001**	**0.002**	**0.0005**	**0.004**	**0.0002**
I130T/+ : G60S/+	0.189	0.118	0.783	0.287	0.083	0.080	0.176	0.120	0.515	0.179
3 Months	Whole Skull		Neural Crest		Mesoderm		Intramembranous		Endochondral	
	Gen	Sex	Gen	Sex	Gen	Sex	Gen	Sex	Gen	Sex
WT-G60S : WT-I130T	**0.0001**	**0.0001**	**0.0001**	**0.0001**	**0.0001**	**0.0001**	**0.0001**	**0.0001**	**0.0001**	**0.0001**
WT-G60S : G60S/+	**0.0001**	**0.005**	**0.0001**	**0.04**	**0.0001**	**0.0001**	**0.0001**	**0.038**	**0.0001**	**0.0001**
WT-I130T : I130T/+	**0.0001**	**0.0001**	**0.0001**	**0.0001**	**0.0001**	**0.0001**	**0.0001**	**0.0001**	**0.0001**	**0.0001**
I130T/+ : G60S/+	**0.0003**	**0.004**	**0.0003**	**0.027**	**0.0001**	**0.0001**	**0.0003**	**0.01**	**0.0001**	**0.0002**

3.2 Mean skull shape is significantly different in mutant compared to wildtype mice and this shape difference is similarly localized in both mutant strains

Shape comparisons between mutants and their wildtype littermates were performed via MANOVA using the proc.D function in the *geomorph* package in R (Adams, et al., 2016). At P0, significant shape differences were present between each mutant and their wildtype littermates for the whole skull and all sub-regions, though these shape differences were greatest between G60S/+ mice and their wildtype littermates (Table 1). Despite the use of centered data to account for mouse strain, significant shape differences were noted between the two wildtype groups for structures derived from mesoderm and those formed through intramembranous ossification (Table 1). To highlight the distribution and severity of these shape differences, heat morphs were constructed to compare the mean phenotypes in a pairwise fashion between mouse groups (Figure 4A). The biggest differences in shape between both mutants and their wildtype littermates were localized to sutural regions of the bones of the cranial vault and face, though these differences were greatest between G60S/+ mice and their wildtype littermates. The heat morphs demonstrate that while the skull phenotype was more severe in G60S/+ mice than in I130T/+ mice, shape anomalies for both mutants were similarly localized.

At 3 months, skull shape differences among all mouse genotypes were statistically significant for the whole skull and all regional subsets (Table 1). The main effects of altered Cx43 function on skull shape were observed in bones of the anterior face, the zygomatic arches and the temporal bones (Figure 4B). Similar to P0 mice, differences in skull shape between G60S/+ mice and their wildtype littermates were more severe than those observed between I130T/+ mutants and their wildtype littermates, but the structures affected were similar in both mutant mice at 3 months (Figure 4B).

To determine the effects of sex on skull shape, we included sex as a factor in our two-way MANOVA for shape comparisons among genotypes. Significant sex effects for shape were present in I130T/+ mice, but not in the G60S/+ mutants at P0 (Table 1). At 3 months, significant sex effects were found for all genotypes, for the whole skull and all

regional subsets. However, no significant sex-by-genotype interactions were found, indicating that these mutations did not modulate skull shape dimorphism.

To further compare the magnitude and direction of shape change between each mutant and their respective wildtype littermates, we performed trajectory analyses. Our results largely confirmed our findings from our shape MANOVAs and heat morphs. At P0, the magnitude of difference in skull shape between G60S/+ mutants and their wildtype littermates was significantly greater than the difference between I130T/+ mice and their wildtype littermates for measures of whole skull as well as mesoderm-derived structures and intramembranously ossified bones, as indicated by the length of the arrows (Figure 5A, B). Additionally, our trajectory analyses showed that the direction of shape differences between G60S/+ mutants and their wildtype littermates at P0 was significantly different than the direction of those measured between I130T/+ mutants and their wildtype controls for the whole skull, mesoderm, and intramembranous subsets (Figure 5A, B). These regional effects indicate that the mesoderm-derived cranial vault was more heavily affected in G60S/+ mice than in I130T/+ mice. While our trajectory analyses indicated that there were significant differences in the direction of shape change between mutants, our trajectory findings align well with our heat morph visualizations of shape change; that is, the greatest differences in mutant skull shape were localized to the cranial vault and G60S/+ mice have the most extreme phenotypic effect (Figure 4A).

At 3 months, the magnitude of shape difference between G60S/+ and their wildtype littermates was significantly greater than that observed between I130T/+ mice and their wildtype controls for the whole skull and all regional subsets (Figure 5A, C). The direction of shape change was also significantly different for G60S/+ and I130T/+ mice for whole skull shape as well as all regional subsets. However, while statistical differences in direction of shape change were noted between the G60S/+ and wildtype and I130T/+ and wildtype comparisons, the direction of shape change was broadly similar for both mutants (Figure 5A, C) indicating that localization of shape differences was largely the same in G60S/+ and I130T/+ mice at 3 months.

Collectively, our findings demonstrate that both mutations significantly affected skull shape at P0 and 3 months, though G60S/+ mice displayed more severely disrupted craniofacial morphology. Additionally, skull shape differences were similarly localized in both mutants compared to their wildtype littermates, suggesting that both mutations affect similar processes of skull development.
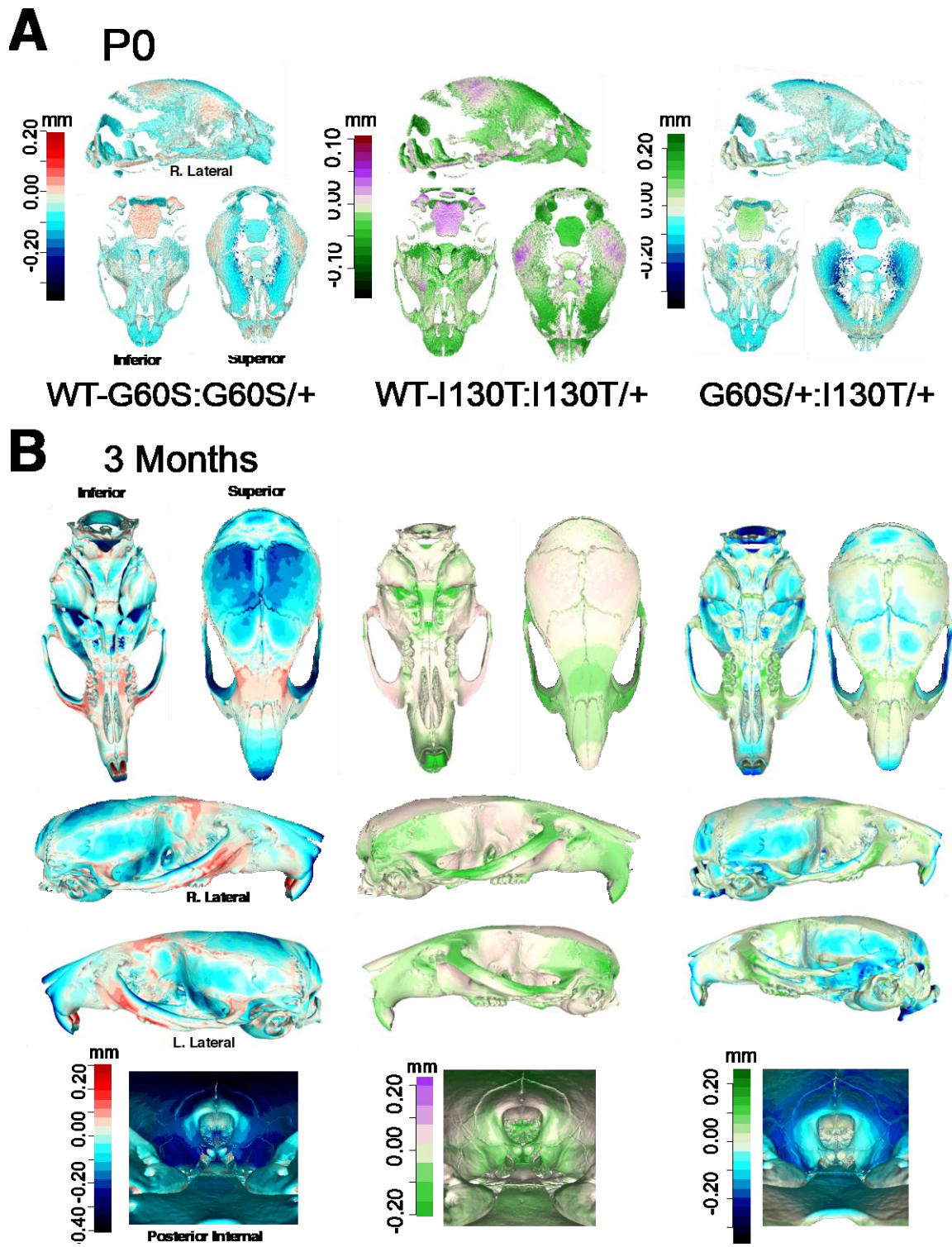
Figure 4 Heat morphs indicate that shape differences between mutant and wildtype mice are similarly localized in both mutant strains.

Heat morphs represent differences in mean skull shape between genotypes at P0 (A) and 3 months (B). Colouration reflects the differences of each genotype from the pooled group average. In the comparison between G60S/+ and their wildtype littermates, red highlights structures that are different in wildtype mice compared to the group mean, whereas blue indicates traits that have a different shape in G60S/+ compared to the group mean. For the comparison between the I130T/+ mutants and their wildtype littermates, purple colouration highlights differences noted for wildtype mice and green indicates differences between I130T/+ mice and the group mean. Finally, for the comparison between G60S/+ and I130T/+ mutants, structures that were most different in G60S/+ mice are coloured in blue and those traits most different in I130T/+ mice compared to the group mean are shown in green.

Trajectories of Shape Change

A

P0

3 Months

Mag. p<0.0001
Dir. p<0.0001

Mag. p<0.005
Dir. p<0.004

● WT-G60S ● G60S/+ ● WT-I130T ● I130T/+

B P0

| Neural Crest | Mesoderm | Intramembranous | Endochondral |

Mag. p<0.469
Dir. p<0.098

Mag. p<0.0003
Dir. p<0.006

Mag. p<0.007
Dir. p<0.006

Mag. p<0.004
Dir. p<0.144

C 3 Months

| Neural Crest | Mesoderm | Intramembranous | Endochondral |

Mag. p<0.0001
Dir. p<0.0001

Mag. p<0.0001
Dir. p<0.0001

Mag. p<0.0001
Dir. p<0.0001

Mag. p<0.0001
Dir. p<0.0001

Figure 5 Magnitude of shape differences between G60S/+ mice and wildtype is greater than shape differences between I130T/+ mice and wildtype.

A: Results from trajectory analyses between each mutant and their wildtype littermates at P0 and 3 months. B: Results from trajectory analyses between mutants and wildtype mice for each regional subset at P0. C: Results from trajectory analyses between mutants and wildtype mice for each regional subset at 3 months. Significance of difference in magnitude (Mag) and direction (Dir) between G60S/+ mutants and their wildtype littermates and I130T/ + mice and their wildtype control are indicated for each comparison. Large circles represent mean shape for each genotype (A-C), and small circles represent individual mice (A).

3.3 Skull shape variation is increased in G60S/+ but not I130T/+ mutant mice

Skull shape variation was assessed and compared between genotypes via pairwise comparisons using the morphol.disparity function in the R package *geomorph* and visualized using scatterplots of PCA scores. At P0, G60S/+ mutants had significantly greater shape variation than their wildtype controls in all regions of the skull except for structures formed through endochondral ossification (Table 2). These results are supported by 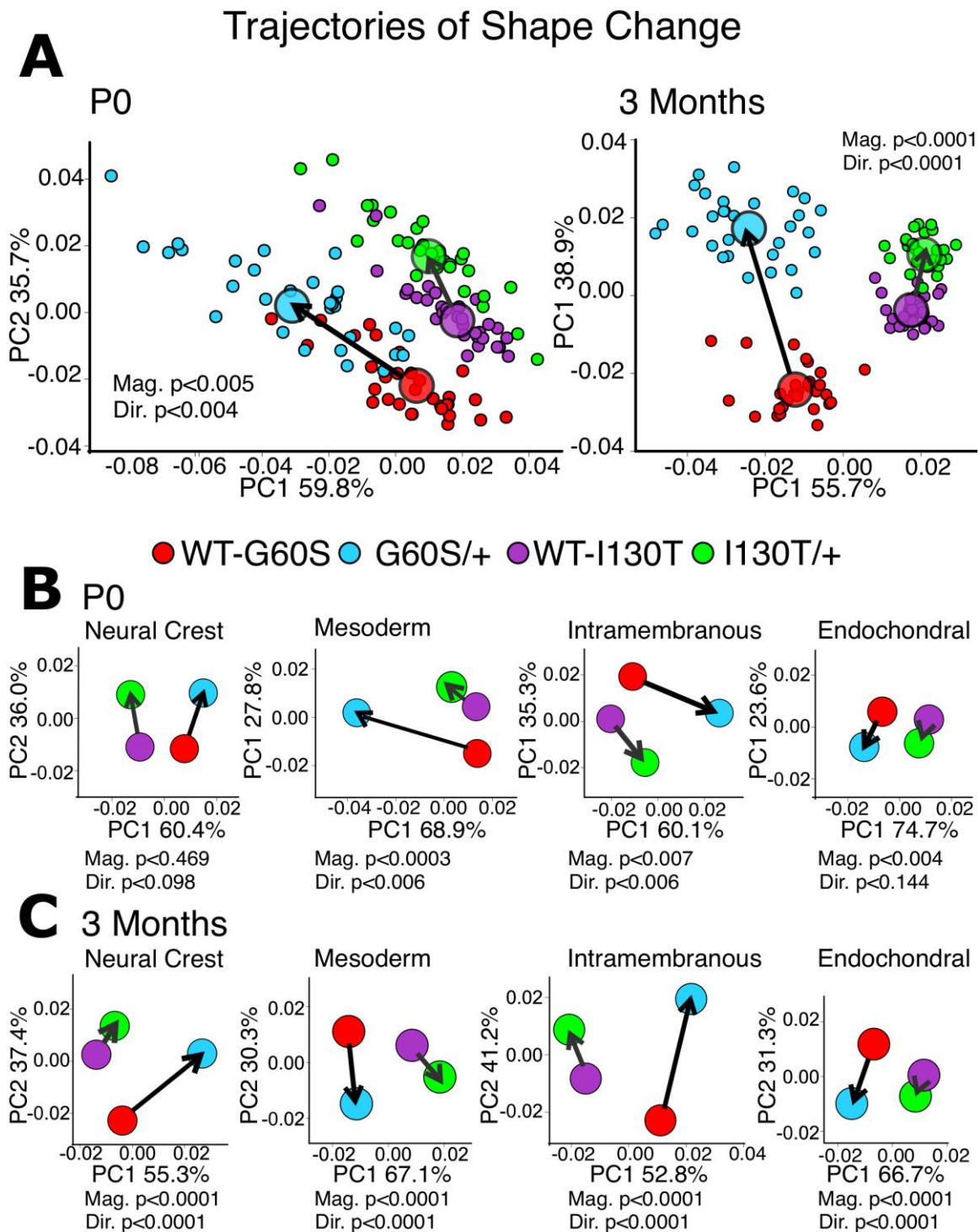the greater spread of PC scores across PC1 and PC2 for G60S/+ mice compared to wildtype controls (Figure 6A, B). Conversely, skull shape variation was unaffected in I130T/+ mutants at P0. Moreover, variation of the whole skull as well as mesoderm-derived, intramembranous bone was greater in G60S/+ mutants compared to I130T/+ mice at P0. These findings are consistent with mean shape differences between mutant mice at birth, wherein the mesoderm-derived bones of the cranial vault had a more severe phenotype in the G60S/+ mice compared to I130T/+ mutants (Figure 4A).

At 3 months, skull shape of G60S/+ mutants was significantly more variable than that of their wildtype littermates for the whole skull and all regional subsets (Table 2). As noted at P0, skull shape variation in I130T/+ mice was not significantly different from that of their wildtype controls at 3 months. Additionally, at 3 months, G60S/+ mutant skulls were significantly more variable than I130T/+ mouse skulls for the whole skull and for all regional subsets. Visualization of skull shape variation using scores from our PCA shows that the distribution of G60S/+ mice was distinct from the other three genotypes along PC1, and also demonstrates that G60S/+ mice had the greatest variation along PC2

(Figure 6A, C). Skull reconstructions of mice that fall at the extreme ends of PC1 indicate that variation along this axis was related to changes in cranial vault width-to-length ratio, where mutants had longer frontal and nasal bones and more narrow cranial vaults compared to wildtype mice (Figure 6A). Variation along PC2 appears to be driven by asymmetric curvature of the facial skeleton found in the G60S/+ mutants (Figure 6A).

Together our analyses of skull shape variation indicated that both P0 and 3-month G60S/+ mutants have increased variation compared to WT-G60S littermates. Interestingly, the I130T/+ mice did not have increased skull shape variation compared to their wildtype littermates at either age. Given that Cx43 channel function is reduced by approximately 50% in I130T/+ mice and approximately 80% in G60S/+ mice (Flenniken, et al., 2005; McLachlan, et al., 2008; Stewart, et al., 2013), our results indicate that the fidelity of skull development is robust to a ~50% reduction in Cx43 function but is compromised at ~80% reduction.

Table 2 Pairwise Comparisons of Skull Shape Variance Between Genotypes at P0 and 3 Months

| P0	Skull	Neural Crest	Mesoderm	Intramembranous	Endochondral
WT-G60S : WT-I130T	0.767	0.81	0.802	0.772	0.804
WT-G60S : G60S/+	**0.0002**	**0.021**	**0.0001**	**0.0002**	0.057
WT-I130T : I130T/+	0.121	0.498	0.069	0.136	0.104
I130T/+ : G60S/+	**0.012**	0.07	**0.017**	**0.009**	0.602
3 Months	Skull	Neural Crest	Mesoderm	Intramembranous	Endochondral
WT-G60S : WT-I130T	**0.012**	**0.019**	**0.016**	**0.029**	**0.001**
WT-G60S : G60S/+	**0.0001**	**0.0001**	**0.003**	**0.0001**	**0.0007**
WT-I130T : I130T/+	0.528	0.605	0.379	0.617	0.340
I130T/+ : G60S/+	**0.0001**	**0.0001**	**0.0001**	**0.0001**	**0.0001**
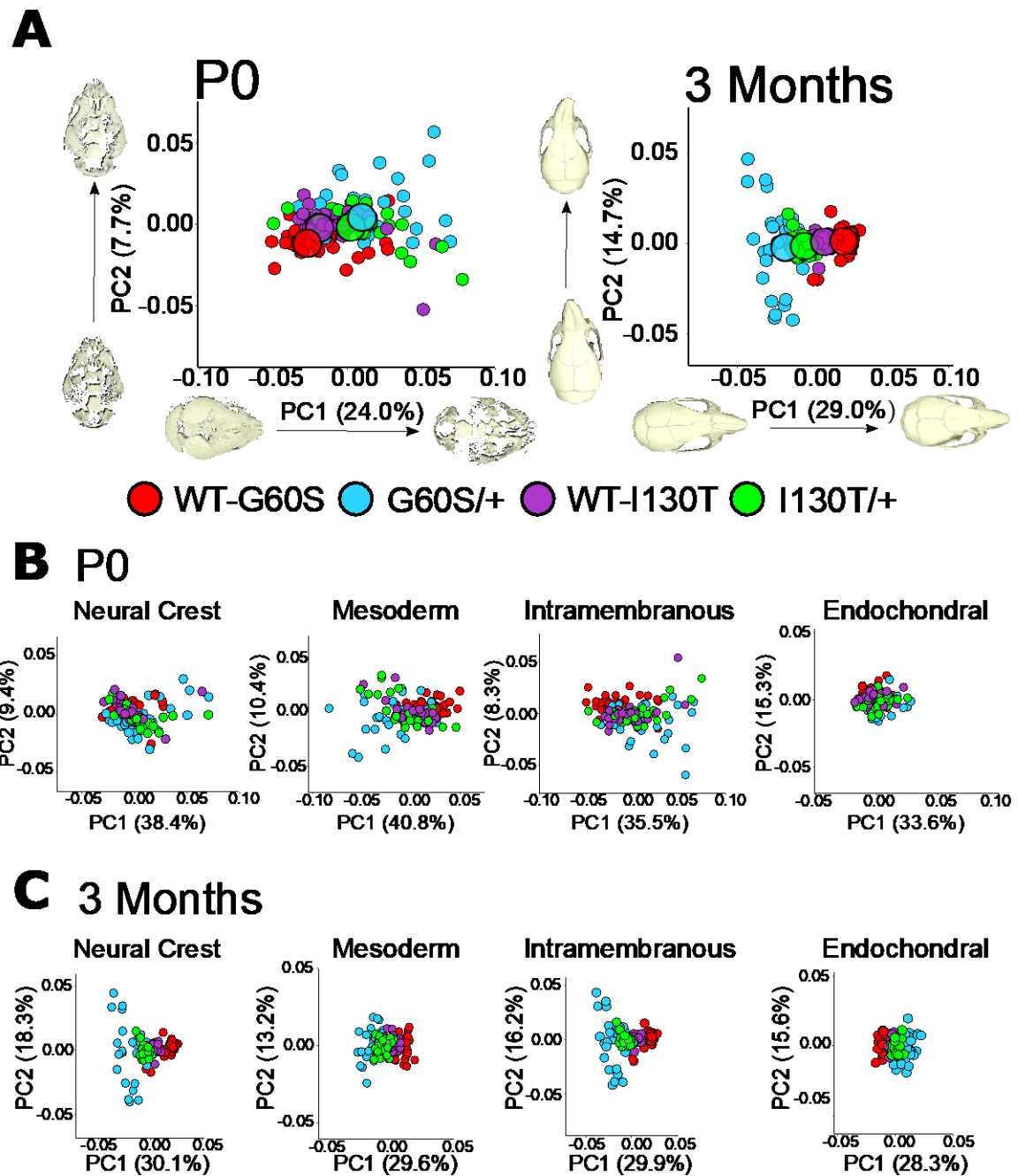
Figure 6 Skull shape variation is greatest in G60S/+ mice at P0 and 3 months.

A: Shape variation is depicted using scatterplots of scores for the first two principal components (PC1 and PC2) for all genotypes for landmarks that represent the whole skull at P0 and 3 months. Micro-CT skull reconstructions represent mice at the extreme ends of PC1 and PC2. B: Shape variation for regional subsets of the skull at P0 depicted using scatterplots of PC1 and PC2. C: Shape variation for regional subsets of the skull at 3 months depicted using scatterplots of PC1 and PC2. Small circles represent individual mice, and large circles represent genotype means.

3.4 Fluctuating asymmetry of the skull is greater in both mutants compared to wildtype at P0, whereas only G60S/+ mice have elevated fluctuating asymmetry at 3 months

Another measure of phenotypic variation is fluctuating asymmetry (FA), which describes the distribution of the random deviation from perfect bilateral symmetry in symmetrical structures (Van Valen, 1962). Greater measures of FA indicate decreased developmental stability. To determine if FA is affected by Cx43 function, FA was measured for the whole skull and each regional subset using the bilat.symmetry function in the *geomorph* package for R, and compared among genotypes using the morphol.disparity function (Adams, et al., 2016). At P0, both mutants had significantly greater FA than their respective wildtype littermates for the whole skull and all regional subsets except for bone derived through endochondral ossification (Table 3, Figure 7A, B). Heat morphs were created to visualize differences in the FA component of skull shape data between genotypes (Figure 8A). These morphs demonstrate that FA was similarly localized to the intramembranous bones of the cranial vault in both mutants at birth.

At 3 months, G60S/+ mice showed significantly greater FA of the whole skull and all regional subsets, whereas FA was unaffected in I130T/+ mice (Table 3, Figure 4A, C). G60S/+ mice also had significantly greater FA than I130T/+ mice for all regions of the skull. These results align with our shape variation comparisons, wherein variance was significantly increased in G60S/+ mutant skulls, but not I130T/+ skulls. While very little FA was measured in 3-month I130T/+ mice, localization of FA within the skull was similar for both mutants, as illustrated by our heat morphs (Figure 8B). In both mutants,

FA was greatest in bones of the posterior cranial vault, the anterior face, and the lateral portion of the frontal bones.

In short, FA was significantly increased in both mutants compared to their wildtype littermates for skull structures of the cranial vault and face formed through intramembranous ossification at P0. However, at 3 months, only G60S/+ mutants had increased FA compared to wildtype littermates. These results are similar to our findings for shape variation, at least for our adult mice. Specifically, developmental stability of the skull, as indicated by levels of FA, appears to be robust to ~50% reduction in Cx43 function but not ~80% reduction in adult mice.

Table 3 Pairwise Comparisons of Fluctuating Asymmetry Between Genotypes at P0 and 3 Months

P0	Skull	Neural Crest	Mesoderm	Intramembranous	Endochondral
WT-G60S : WT-I130T	0.1614	0.3837	0.1927	0.1476	0.7073
WT-G60S : G60S/+	**0.0001**	**0.0035**	**0.0001**	**0.0001**	0.7908
WT-I130T : I130T/+	**0.0006**	**0.018**	**0.0015**	**0.0006**	0.373
I130T/+ : G60S/+	0.364	0.6023	0.3904	0.2628	0.0788
3 Months	Skull	Neural Crest	Mesoderm	Intramembranous	Endochondral
WT-G60S : WT-I130T	0.1871	0.1546	0.4569	0.1229	0.8898
WT-G60S : G60S/+	**0.0001**	**0.0001**	**0.0001**	**0.0002**	**0.0001**
WT-I130T : I130T/+	0.1164	0.1027	0.2818	0.1527	0.1053
I130T/+ : G60S/+	**0.0002**	**0.0002**	**0.0004**	**0.0003**	**0.0001**
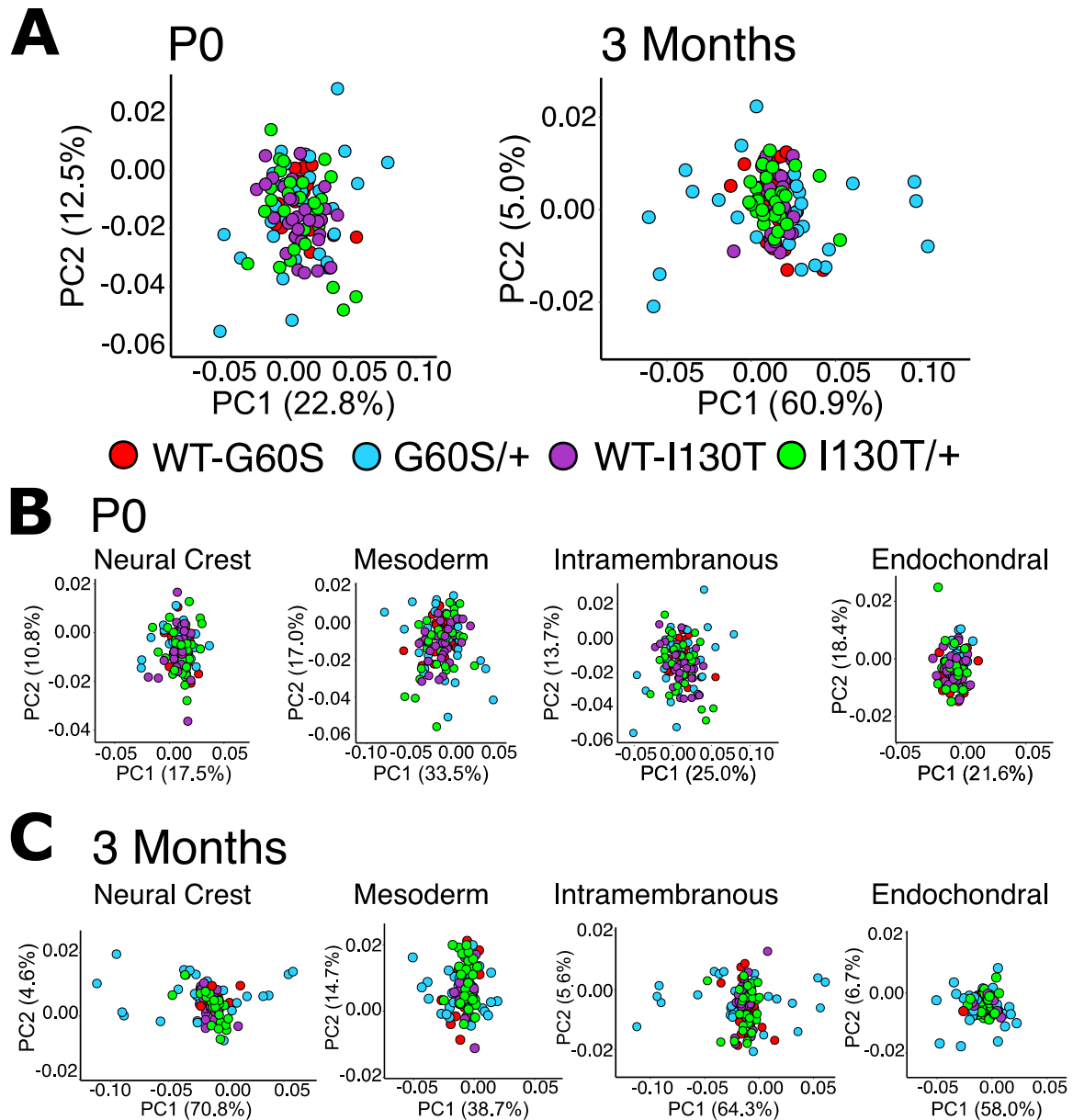
Figure 7 Both mutants demonstrate elevated FA at P0 compared to wildtype mice, whereas only G60S/+ mice have elevated FA at 3 months.

A: FA is depicted using scatterplots of scores for the first two principal components (PC1 and PC2) determined using the FA component from superimposed landmark data for the whole skull at P0 and 3 months. B: FA for regional subsets of the skull at P0 depicted using scatterplots of PC1 and PC2. C: FA for regional subsets of the skull at 3 months depicted using scatterplots of PC1 and PC2.

A P0

Superior   Inferior

L. Lateral

R. Lateral

WT-G60S:G60S/+   WT-I130T:I130T/+   G60S/+:I130T/+

B 3 Months

Superior   Inferior

L. Lateral

R. Lateral

PosteriorInternal

Figure 8 Heat morphs indicate that FA differences between mutant and wildtype mice are similarly localized in both mutant strains.

Heat morphs represent differences FA at P0 (A) and 3 months (B). Colouration reflects the differences of each genotype from the pooled group average. In the comparison between G60S/+ and their wildtype littermates, red highlights structures that are different in wildtype mice compared to the group mean, whereas blue indicates traits that have a different shape in G60S/+ compared to the group mean. For the comparison between the I130T/+ mutants and their wildtype littermates, purple colouration highlights differences noted for wildtype mice and green indicates differences between I130T/+ mice and the group mean. Finally, for the comparison between G60S/+ and I130T/+ mutants, structures that were most different in G60S/+ mice are coloured in blue and those traits most different in I130T/+ mice compared to the group mean are shown in green.

3.5 Patterns of skull covariation are similar among all genotypes but the strength of covariation in G60S/+ mice is significantly reduced

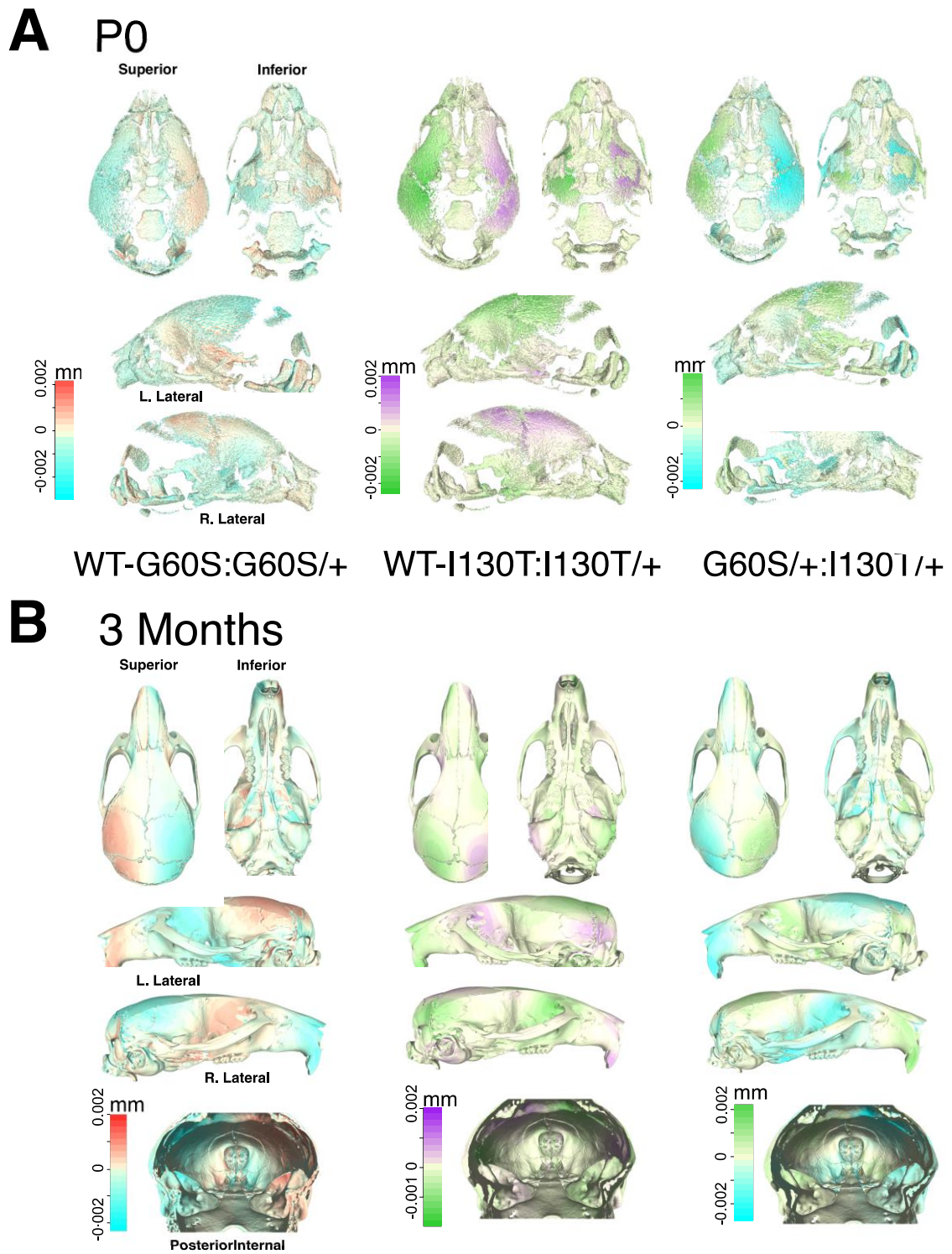To further understand how the patterning of phenotypic variation compared among genotypes, we measured and compared skull covariation among all mouse groups using group-mean centered two-block PLS analyses. Specifically, we analysed covariation between skull structures derived from neural crest and mesoderm and between skull bones formed through intramembranous and endochondral ossification. At P0, covariation between neural crest and mesoderm traits was high and statistically significant for all genotypes (range of rPLS: 0.78-0.88). Covariation between structures formed through intramembranous and endochondral ossification was likewise strong and statistically significant for all genotypes (range of rPLS: 0.82-0.93). Comparisons of the strength of covariation among genotypes performed using effect size demonstrated similar covariation for all genotypes for both sets of comparisons (mode of ossification and tissue origin) (Table 4). These results were visualized through scatterplots of scores for the first PLS axes (PSL1) for the blocks of our ossification mode comparison and the blocks for our tissue origin comparison (Figure 9A). Scores for PLS1 overlapped among genotypes and showed a clustering at the positive end of the intramembranous and endochondral axes in the ossification mode comparison, and mesoderm and neural crest

axes in the tissue origin comparison. While all genotypes demonstrated a strong correlation among these blocks of data, skull shape differed along each axis. At the positive end of the axes for both comparisons, P0 skulls were more developed than those found at the negative end of the axes. The most overt differences in development were noted in the bones of the cranial vault and face, but also included bones of the cranial base, particularly the anterior portion of the cranial base.

At 3 months, covariation between regional subsets was even stronger than that observed at P0. Covariation as measured by PLS between intramembranously and endochondrally ossified structures was very high and statistically significant for all genotypes (range of rPLS: 0.82-0.94) and was likewise strong and statistically significant for all mouse groups between neural crest- and mesoderm-derived traits (range of rPLS: 0.84-0.95). While all genotypes demonstrated strong and significant covariation between blocks of data, comparisons among genotypes revealed that the strength of covariation for both sets of blocks (mode of ossification and tissue origin) was significantly weaker in 3-month G60S/+ mice compared with their wildtype littermates and compared with I130T/+ mutants (Table 4). Visualization of scores for PLS1 for intramembranous and endochondral blocks and for neural crest and mesoderm blocks confirmed our statistical findings (Figure 9B). For both comparisons, all genotypes demonstrated a strong and similar covariation between blocks of data, though the G60S/+ mice had a greater spread around the main axis. The PLS1 scores formed discrete clusters among genotypes for both two-block comparisons and highlight the shape differences among genotypes, particularly the shape differences observed in G60S/+ mice. For both mode of ossification and tissue origin comparisons, the strong covariation appeared to arise from changes in neurocranial width (cranial base and cranial vault) and face length, with G60S/+ mice tending to have a wide cranial vault and cranial base and short facial skeleton (Figure 9B).

Collectively, our results indicated strong covariation among skull structures derived from neural crest and mesoderm and among traits formed through intramembranous and endochondral ossification for all mouse groups at P0 and 3 months. However, at 3 months, while still significantly high, the strength of covariation between these blocks of

data was significantly reduced in G60S/+ mutants compared to all other genotypes. These findings suggested that the structure of variation is altered in 3-month G60S/+ mutants.

Table 4 . Comparisons of Strength of Covariation Between Regional Subsets of the Skull Among Genotypes at P0 and 3 Months

P0	Neural Crest & Mesoderm		Intramembranous & Endochondral	
	Effect Size	P-value	Effect Size	P-value
WT G60S : WT I130T	0.6359	0.2624	1.431	0.0762
WT G60S : G60S/+	0.1381	0.4451	0.03488	0.4861
WT I130T : I130T/+	0.1198	0.4523	0.3669	0.3569
I130T/+ : G60S/+	0.7428	0.2288	1.0220	0.1534
3 Months	Neural Crest & Mesoderm		Intramembranous & Endochondral	
	Effect Size	P-value	Effect Size	P-value
WT G60S : WT I130T	0.1378	0.4452	0.6370	0.2621
WT G60S : G60S/+	2.468	**0.0068**	2.297	**0.0108**
WT I130T : I130T/+	0.7513	0.2262	1.432	0.0760
I130T/+ : G60S/+	2.994	**0.0014**	3.097	**0.0010**
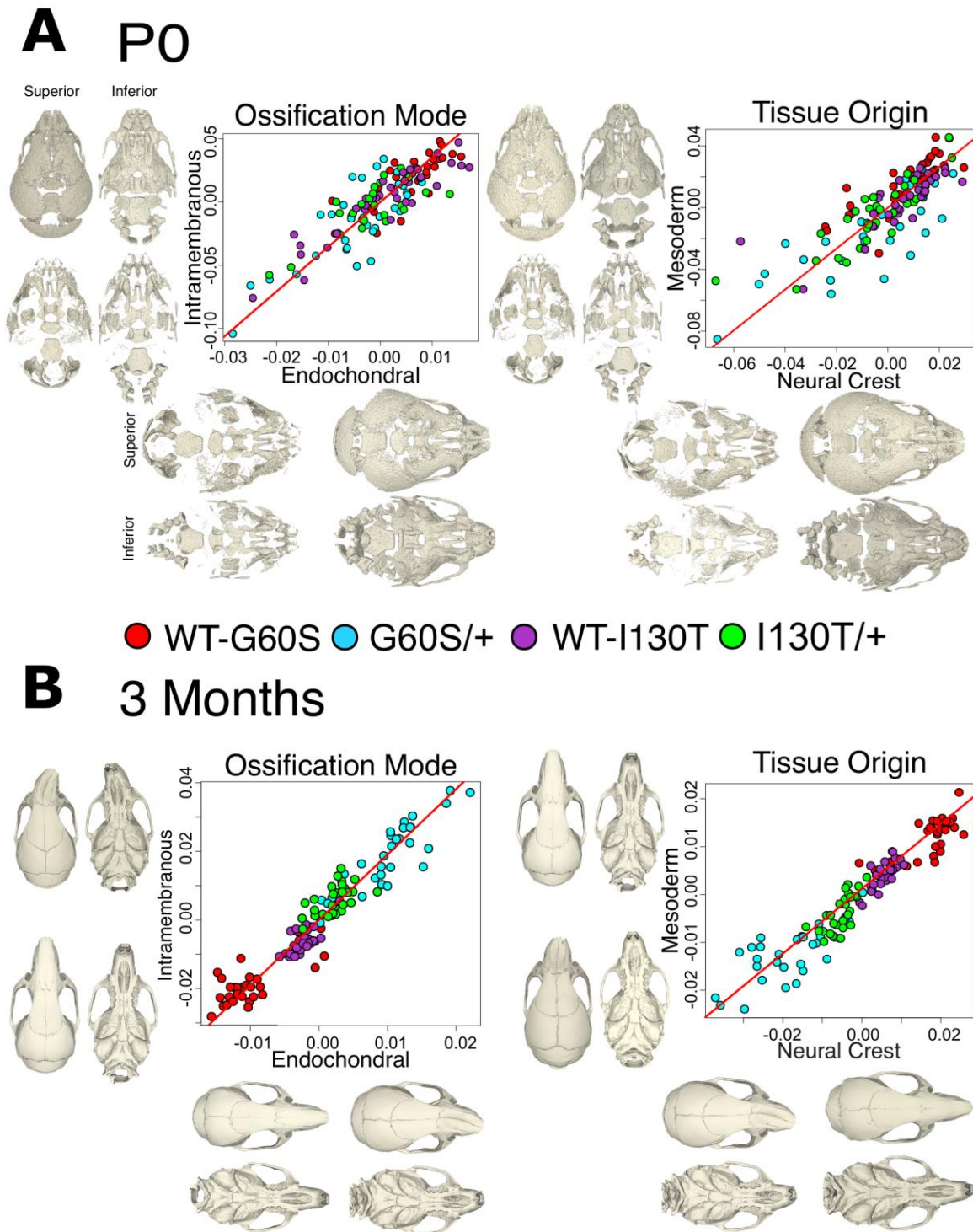
Figure 9 Covariation among regional subsets of the skull is strong for all genotypes at P0 and 3 months, though G60S/+ mutants have significantly weaker covariation than wildtype and I130T/+ mice at 3 months.

Covariation between blocks of landmarks that represent structures formed through different modes of ossification (endochondral and intramembranous) and derived from different tissue origins (neural crest and mesoderm) is represented using scatterplots of scores for the first axis from two-block partial least squares analyses (PLS1) at P0 (A) and 3 months (B). Micro-CT skull reconstructions in superior and inferior view represent mice at the extreme ends of PLS1 for each comparison.

Chapter 4

4   Discussion

This study explored the prediction that phenotypic variability can arise through embedded properties of development by investigating whether this concept extends to a gene that plays an active, though not crucial, role in skull development. Specifically, it investigated the role of Cx43 in modulating developmental variability of the skull by quantitatively measuring and comparing skull shape and size, variation, FA, and covariation among mice with two different *Gja1* mutations (and subsequent different reductions in Cx43 gap junction channel function) and their wildtype littermates. We found that skull shape and size in both newborn and 3-month mice were significantly different in both mutant mice compared to wildtype, and while the skull phenotype was more severe in the G60S/+ mutants, differences in mutant skull shape were similarly localized. Skull shape variation, however, was significantly increased in the G60S/+ mutants only. Fluctuating asymmetry was significantly greater in both mutants compared to wildtype at birth, but by 3 months, only the G60S/+ mice displayed greater FA compared to their wildtype littermates. Covariation between skull regions formed through endochondral and intramembranous ossification and between traits derived from neural crest and mesoderm was significant and very strong for all genotypes at birth and 3 months. However, covariation was significantly less strong between these regional subsets in G60S/+ mice at both ages compared to other genotypes. Together these findings indicate that both mutations target the same developmental processes and are sufficient to cause a shift in mean phenotype, and that Cx43 can modulate phenotypic variation of the skull, but only if protein function is reduced beyond a relatively permissive threshold.

Skull shape differences in mutants compared to wildtype mice were similarly localized in G60S/+ and I130T/+ mice at birth and 3 months, though the phenotypic effects were more severe in G60S/+ mutants. At birth these shape differences were largely concentrated in regions of active ossification such as the sutural edges of the bones of the cranial vault and face. These findings are consistent with the well-established role that Cx43 plays in osteoblast differentiation and bone development (Lecanda, et al., 2000;

Chung, et al., 2006; Dobrowolski, et al., 2007; McLachlan, et al., 2008; Watkins, et al., 2011; Jarvis, et al., 2020), and indicate that the differences in skull shape at P0 may be due to delayed osteoblast differentiation. At 3 months, differences in shape between wildtype and mutant mice are more severe than those observed in newborns, aligning well with previous work from our lab (Jarvis, et al., 2020). As with newborn mice, at 3 months both mutants differ in skull shape similarly compared to their wildtype littermates. However, these differences are now localized to the anterior face, the palate near the molars, the zygomatic arches, and the temporal bones. These regions all coincide with areas of mechanical stimulation through chewing (Baverstock, Jeffery, & Cobb, 2013), and indicate that shape differences in 3-month mutants may be due to altered mechanotransduction in bone. Indeed, several studies have demonstrated the role of Cx43 in bone mechanotransduction (Alford, Jacobs, & Donahue, 2003; Jiang, Siller-Jackson, & Burra, 2007; Taylor, et al., 2007; Watkins, et al., 2011; Grimston, Watkins, Stains, & Civitelli, 2013; Plotkin, Speacht, & Donahue, 2015). While most of the shape differences between mutant mice were similarly localized, at 3 months, the G60S/+ mice displayed overt differences in the shape of the posterior cranial vault compared to wildtype that were not observed in I130T/+ mice. Additionally, our trajectory analyses indicated statistically significant differences in direction of phenotypic change between mutants, though the trajectory of shape difference was broadly similar in G60S/+ and I130T/+ mice. These differences in skull shape are likely due to differences in genetic background, as genetic background has been shown to be able to strongly affect the phenotypic consequences of the same mutation (Percival, et al., 2017). In general, even though these mutant mouse strains are on different genetic backgrounds, G60S/+ and I130T/+ mutants displayed very similar skull phenotypes that correspond with the known roles of Cx43 in bone development and remodeling. Thus, we suggest that both mutations act on similar processes of skull development through reduced Cx43 channel function.

Skull shape variation was increased in G60S/+ newborn and 3-month mice compared to wildtype, suggesting that Cx43 can play a role in modulating phenotypic variation. I130T/+ mice did not show increased levels of shape variation despite displaying changes in mean skull shape compared to wildtype. These findings are consistent with early studies that demonstrated that more extreme phenotypes tend to have increased shape

variation (Waddington, The Strategy of the Genes, 1957; Scharloo, 1991). Moreover, our results indicate a threshold effect of Cx43 function on skull shape variation. Cx43 channel function is reduced to ~20% in G60S/+ mice and to ~50% in I130T/+ mutants compared to wildtype (Flenniken, et al., 2005; McLachlan, et al., 2008; Stewart, et al., 2013), and thus, while reduction to ~50% Cx43 function is sufficient to shift mean shape, it is not sufficient to disrupt the fidelity of development. This threshold effect on mean skull shape and shape variation has been previously demonstrated in relation to gene dosage. For example, Young and colleagues discovered a nonlinear relationship between SHH ligand concentration and upper jaw formation in chicks, where small changes in concentration below a threshold led to dramatic phenotypic outcomes, whereas changes in concentration above the threshold yielded relatively minor differences in jaw shape (Young et al., 2010). Similarly, a recent study demonstrated that *Fgf8* dosage relates nonlinearly with mouse craniofacial shape variation with no changes in shape variation until *Fgf8* expression falls below 40% of that found in wildtype mice (Green, et al., 2017). Further analyses indicated that the nonlinear relationship between *Fgf8* and craniofacial phenotype was caused by a nonlinear response in downstream genes to changes in *Fgf8* dosage. A possible explanation for the threshold effect for phenotypic variation found in this study is the role that Cx43 gap junctions can play in amplifying cell signaling. Gap junctions exchange second messengers to adjacent cells that converge on downstream signaling pathways. Each target cell can then pass these second messengers onto neighbouring cells, creating a cascade effect and amplifying the original stimulus (Lima et al., 2009; Niger, et al., 2012; Buo & Stains, 2014). Thus, it is possible that normal Cx43 cell signaling exceeds physiological needs and provides built-in functional redundancy. However, when Cx43 function falls below a threshold, the resultant gap junction-facilitated signaling cascade may be insufficient to trigger downstream pathways. While this explanation is consistent with our current understanding of the role of Cx43 in bone development and homeostasis, it remains to be demonstrated experimentally. Additionally, cell signaling through Cx43 hemichannels could contribute to our findings, though currently it is difficult to disentangle the effects of Cx43 gap junctions and hemichannels on phenotypic outcomes (Riquelme et al., 2020).

The effects of Cx43 function on skull FA appeared to change with age. At birth, both G60S/+ and I130T/+ mice had elevated levels of FA compared to their wildtype littermates, whereas only G60S/+ mice had increased FA at 3 months. Thus, at P0, a reduction of Cx43 function to ~50% is sufficient to reduce developmental stability, whereas at 3 months, there is a greater tolerance for reduced Cx43 function. We consider both shape variation and FA to be indicators of phenotypic variability, with shape variation representing a more global measure and FA a localized indicator. The differential effect of Cx43 on these measures at P0 demonstrates the importance of developmental scale and timing when studying the developmental determinants of variation. Indeed, several studies have tested the congruence between shape variation and FA, and to date, no consensus has been reached, leading to the suggestion that variation at these different phenotypic scales is modulated by separate developmental processes (Klingenberg & McIntyre, 1998; Debat et al., 2000; Willmore, Klingenberg, & Hallgrímsson, 2005; Breno, Leirs, & Van Dongen, 2011; Varón-González et al., 2019). Our results indicate that congruence between shape variation and FA could be context-specific, rather than all or nothing. At P0, mouse skulls are actively undergoing ossification. Given that cell-cell communication through Cx43 gap junctions can amplify cell signaling that acts on downstream pathways of bone formation, it is reasonable that relatively small changes in Cx43 function could lead to highly localized changes in ossification during this developmental period of high activity (Lima et al., 2009; Niger, et al., 2012; Buo & Stains, 2014). On the other hand, at 3 months, Cx43 contributes to bone remodeling (Watkins et al., 2011; Grimston et al., 2013; Stains et al., 2014). It is possible that processes of bone remodeling are less sensitive to Cx43 function at the highly localized scale, such that FA is only elevated at a much lower threshold for Cx43 channel function. Ultimately, our results indicate that Cx43 channel function does contribute to developmental stability of the skull.

Phenotypic covariation describes how variation is structured within a trait and is a measure of morphological integration (Olson & Miller, 1958; Cheverud, 1982; Hallgrímsson, Willmore, & Hall, 2002). Morphological integration coordinates development of traits that serve common functional demands. While measures of integration are not often included as a metric of phenotypic variability, we suggest that

differences in integration within the same species indicate a disruption to developmental fidelity, as these differences could result in adverse functional consequences. Our skull covariation findings further support the suggestion that Cx43 channel function contributes to phenotypic variability via a nonlinear relationship. Covariation between skull traits formed through endochondral and intramembranous ossification and between regions derived from neural crest and mesoderm was very high and statistically significant for all genotypes at P0 and 3 months. However, covariation among skull regions was significantly lower in G60S/+ mice at both ages, whereas covariation within I130T/+ mutants was similar to that of wildtype mice. Thus, as we found for shape variation, Cx43 appears to contribute to morphological integration through a threshold effect.

4.1 Limitations and Future Studies

A limitation of the models used in this study was that the genetic backgrounds of the two mouse models were not consistent, with I130T/+ mice being on a C57BL/6 background and the G60S/+ model bred on the C3H/HeJ strain. While this was statistically accounted for during analysis, the known variable penetrance of the ODDD phenotype means that background effects were likely a factor in those phenotypes observed. In the future ensuring a common murine background between mutants would amend this limitation. Another limitation of these models stems from the loss of Cx43 function being achieved using mutations. In future, using knock-down mouse models would allow for phenotypic analyses to be done at multiple gradations of Cx43 function. This approach could help pinpoint the threshold beyond which variation increases dramatically. Also, the function of Cx43 was not measured for each individual, nor was the amount of *Gja1* expression in each individual measured, so the linearity of Cx43 function to phenotypic variation was generalized using data from previous studies of these mouse models. The expression of other connexins in bone was also not investigated to determine if there was compensation for the loss of Cx43 function.

A clearer understanding of how embedded properties of development modulate phenotypic variability will help address fundamental questions related to evolutionary and developmental biology, but is also clinically relevant. For example, uncovering the

specific developmental consequences that cascade from varying levels of Cx43 gap junction function through to specific phenotypic outcomes would provide a mechanistic explanation for the high phenotypic variability observed in patients with ODDD. Indeed, different clinical presentation among ODDD patient groups with the same mutation underscores the variable penetrance of *GJA1* mutations. Such variable penetrance presents challenges for diagnosis and for attempts to develop effective therapeutic strategies. Further exploration of how embedded processes of development influence mutational effects on phenotype could provide important insight into many developmental diseases.

4.2   Conclusion

Collectively, our results indicate that Cx43 can contribute to phenotypic variability of the skull through a nonlinear relationship between the level of gap junction function and skull morphology. These findings suggest that modulation of craniofacial phenotypic variance through embedded processes of development can extend beyond genes of essential importance in skull development.

Bibliography

Abitbol, J. M., Kelly, J. J., Barr, K. J., Allman, B. L., & Laird, D. W. (2018). Mice harbouring an oculodentodigital dysplasia-linked Cx43 G60S mutation have severe hearing loss. *Journal of Cell Science, 131*(9), jcs214635.

Abitbol, J. M., O'Donnell, B. L., Wakefield, C. B., Jewlal, E., Kelly, J. J., Barr, K., . . . Penuela, S. (2019). Double deletion of Panx1 and Panx3 affects skin and bone but not hearing. *Journal of Molecular Medicine*, 1-14.

Adams, D. C., & Collyer, M. L. (2009). A General Framework for the Analysis of Phenotypic Trajectories in Evolutionary Studies. *Evolution, 63*(5), 1143-1154.

Adams, D. C., & Collyer, M. L. (2016). On the comparison of the strength of morphological integration across morphometric datasets. *Evolution, 70*(11), 2623-2631.

Adams, D. C., & Collyer, M. L. (2018, Jan). Multivariate Phylogenetic Comparative Methods: Evaluations, Comparisons, and Recommendations. *Systematic Biology, 67*(1), 14-31.

Adams, D. C., Collyer, M., Kaliontzopoulou, A., & Sherratt, E. (2016). geomorph: Software for geometric morphometric analyses. *Comprehensive R Archive Network*.

Adams, D. C., Rohlf, F. J., & Slice, D. E. (2013, May 7). A field comes of age: geometric morphometrics in the 21st century. *Hystrix the Italian Journal of Mammalogy, 24*(1), 7-14.

Alford, A. I., Jacobs, C. R., & Donahue, H. J. (2003, Jul 1). Oscillating fluid flow regulates gap junction communication in osteocytic MLO-Y4 cells by an ERK 1/2 MAP kinase-dependant mechanism. *Bone, 33*(1), 64-70.

Baab, K. L., McNulty, K. P., & Rohlf, F. J. (2012, Aug 20). The shape of human evolution: A geometric morphometrics perspective. *Evolutionary Anthropology: Issues, News, and Reviews, 21*(4), 151-165.

Baverstock, H., Jeffery, N. S., & Cobb, S. N. (2013). The morphology of the mouse masticatory musculature. *Journal of Anatomy, 223*(1), 46-60.

Bavia, P. F., Vilanova, L. S., & Garcia, R. C. (2016, Sep-Oct). Craniofacial Morphology Affects Bite Force in Patients with Painful Temporomandibular Disorders. *Brazilian Dentistry Journal, 27*(5), 619-624.

Beaucage, K. L., Xiao, A., Pollmann, S. I., Grol, M. W., Beach, R. J., Holdsworth, D. W., . . . Dixon, S. J. (2014). Loss of P2X7 nucleotide receptor function leads to abnormal fat distribution in mice. *PUrinergic Signal, 10*(2), 291-304.

Bivi, N., Condon, K. W., Allen, M. R., Farlow, N., Passeri, G., Brun, L. R., . . . Plotkin, L. (2012, Feb). Cell autonomous requirement of connexin 43 for osteocyte survival: consequences for endocortical resorption and periosteal bone formation. *Journal of Bone Mineral Research, 27*(2), 374-389.

Bolande, R. P. (1997). Neurocristopathy: Its Growth and Development in 20 Years. *Pediatric Pathology & Laboratory Medicine, 17*(1), 1-25.

Breno, M., Bots, J., & Van Dongen, S. (2013). Heritabilities of directional asymmetry in the fore and hindlimbs of rabbit fetuses. *PloS One, 8*(10).

Breno, M., Leirs, H., & Van Dongen, S. (2011). No relationship between canalization and developmental stability of the skull in a natural population of Mastomys natalensis (Rodentia: Muridae). *Biological Journal of the Linnean Society, 104*(1), 207-216.

Buo, A. M., & Stains, J. P. (2014, Apr 17). Gap junctional regulation of signal transduction in bone cells. *FEBS Letters, 588*(8), 1315-1321.

Cardini, A. (2019). Integration and Modularity in Procrustes Shape Data: Is There a Risk of Spurious Results? *Evolutionary Biology, 46*, 90-105.

Cardini, A., & Elton, S. (2007). Sample size and sampling error in geometric morphometric studies of size and shape. *Zoomorphology, 126*, 121-134.

Caskenette , D., Penuela, S., Lee, V., Barr, K., Beier, F., Laird, D. W., & Willmore, K. E. (2016). Global deletion of Panx3 produ7ces multiple phenotypic effects in mouse humeri and femora. *Journal of Anatomy, 228*(5), 746-756.

Chai, Y., & Maxson, R. E. (2006). Recent advances in craniofacial morphogenesis. *Developmental Dynamics, 235*(9), 2353-2375.

Cheverud, J. M. (1982). Phenotypic, Genetic and Environmental Morphological Integration in the Cranium. *Evolution, 36*(3), 499-516.

Cheverud, J. M. (1996). Developmental integration and the evolution of pleitropy. *American Zoologist, 36*, 44-50.

Chung, D. J., Castro, C. H., Watkins, M., Stains, J. P., Chung, M. Y., Szejnfeld, V. L., . . . Civitelli, R. (2006). Low peak bone mass and attenuated anabolic response to parathyroid hormone in mice with an osteoblast-specific deletion of connexin43. *Journal of Cell Science, 119*(20), 4187-4198.

Clarke, G. M. (1998). The genetic basis of developmental stability. *Heredity, 80*, 562-567.

Collyer, M. L., Sekora, D. J., & Adams, D. C. (2015, Oct 1). A method for analysis of phenotypic change for phenotypes described by high-dimensional data. *Heredity, 115*(4), 357-365.

Dash, S., & Trainor, P. A. (2020). The development, patterning and evolution of neural crest cell differentition into cartilage and bone. *Bone, 137*, 115409.

De Coster, G., Van Dongen, S., Malaki, P., Muchane, M., Alcántara-Exposito, A., Matheve, H., & Lens, L. (2013). Fluctuating Asymmetry and Environmental Stress: Understanding the Role of Trait History. *PLOS ONE, 8*(3), e57966.

de Visser, J. A., Hermisson, J., Wagner, G. P., Meyers, L. A., Bagheri-Chaichian, H., Blanchard, J. L., . . . Whitlock. (2003, Sep). Perspective: Evolution and detection of genetic robustness. *Evolution, 57*(9), 1959-72.

Debat, V., & David, P. (2001). Mapping phenotypes: canalization, plasticity and developmental stability. *Trends in Ecology & Evolution, 16*(10), 555-561.

Debat, V., Alibert, P., David, P., Paradis, E., & Auffray, J.-C. (2000). Independence between developmental stability and canalization in the skull of the house mouse. *Proceedings of the Royal Society of London Series B: Biological Sciences, 267*(1442), 423-430.

DeLaurier, A., Huycke, T. R., Nichols, J. T., Swartz, M. E., Larsen, A., Walker, C., . . . Kimmel, C. B. (2014). Role of mef2ca in developmental buffering of the zebrafish larval hyoid dermal skeleton. *Developmental Biology, 385*(2), 189-199.

Dobrowolski, R., Sasse, P., Schrickel, J. W., Watkins, M., Kim, J.-S., Rackauskas, M., . . . Willecke, K. (2007). The conditional connexin43 G138R mouse mutant represents a new model of hereditary oculodentodigital dysplasia in humans. *Human Moledcular Genetics, 17*(4), 539-554.

D'Souza, R. N., Ruest, L. B., Hinton, R. J., & Svoboda, K. K. (2010). Development of the Craniofacial Complex. In F. Bronner, M. Farach-Carson, & H. Roach, *Topics in Bone Biology* (Vol. 6, pp. 153-181). London: Springer.

Dun, R. B., & Fraser, A. S. (1958). Selection for an Invariant Character -- "Vibrissa Number" -- in the House Mouse. *Nature, 181*(4614), 1018-1019.

Dun, R. B., & Fraser, A. S. (1959). Selection for an Invariant Character, Vibrissa Number, in the House Mouse. *Australian Journal of Biological Sciences, 12*(4), 506.

Ebert, M. S., & Sharp, P. A. (2012). Roles for microRNAs in confering robustness to biological processes. *Cell, 149*(3), 515-524.

Feng, X., & McDonald, J. M. (2011). Disorders of bone-remodeling. *Annual Review of Pathology, 6*, 121-145.

Flenniken, A. M., Osborne, L. R., Anderson, N., Ciliberti, N., Fleming, C., Gittens, J. E., . . . Zh. (2005, Oct). A Gja1 missense mutation in a mouse model of oculodentodigital dysplasia. *Development, 132*(19), 4375-86.

Frelat , M. A., Katina, S., Weber, G. W., & Bookstein, F. L. (2012, Nov 2). Technical note: A novel geometric morphometric approach to the study of long bone shape variation. *American Journal of Physical Anthropology, 149*(4), 628-638.

Gonzalez, P. N., Lotto, F. P., & Hallgrímsson, B. (2014). Canalization and developmental instability of the fetal skull in a mouse model of maternal nutritional stress. *American Journal of Physical Anthropology, 154*(4), 544-553.

Goodenough, D. A., Goliger, J. A., & Paul, D. L. (1996). Connexins, connexons, and intercellular communication. *Annual Review of Biochemistry, 65*(1), 475-502.

Green, R. M., Fish, J. L., Young, N. M., Smith, F. J., Roberts, B., Dolan, K., . . . Hallgrímsson, B. (2017). Developmental nonlinearity drives phenotypic robustness. *Nature Communications, 8*(1), 1970.

Green, R. M., Leach, C. L., Diewert, V. M., Aponte, J. D., Schmidt, E. J., Chevreud, J. M., . . . Hallgrímsson, B. (2019, Dec). Nonlinear gene expression-pehnotype relationships contribute to variation and clefting in the A/WySn mouse. *Developmental Dynamics, 248*(12), 1232-1242.

Grimston, S. K., Watkins, M. P., Stains, J. P., & Civitelli, R. (2013). Connexin43 modulates post-natal cortical bone modeling and mechano-responsiveness. *BoneKEy Reports, 2*, 446.

Hallgrímsson, B., & Lieberman, D. E. (2008, Sep). Mouse models and the evolutionary developmental biology of the skull. *Integrative and Comparative Biology, 48*(3), 373-384.

Hallgrímsson, B., Green, R. M., Katz, D. C., Fish, J. L., Bernier, F. P., Roseman, C. C., . . . Marcucio, R. S. (2019). The developmental-genetics of canalization. *Seminars in Cell & Developmental Biology, 88*, 67-79.

Hallgrímsson, B., Mio, W., Marcucio, R. S., & Spritz, R. (2014, Nov). Let's Face It--Complex Traits Are Just Not That Simple. *PLoS Genetics, 10*(11), e1004724.

Hallgrímsson, B., Willmore, K., & Hall, B. K. (2002). Canalization, developmental stability, and morphological integration in primate limbs. *American Journal of Physical Anthropology, 119*(S35), 131-158.

Hartl , D. L., Dykhuizen, D. E., & Dean, A. M. (1985). Limits of adaptation: the evolution of selective neutrality. *Genetics, 111*(3), 655-74.

Heuzé, Y., Martínez-Abadías, N., Stella, J. M., Arnaud, E., Collet, C., Garcia Fructuoso, G., & Richtsmeier, J. T. (2014). Quantification of facial skeletal shape variation in fibroblast growth factor receptor-related craniosynostosis syndromes. *Birth Defects Research, 100*(4), 250-259.

Hothorn, T., Bretz, F., & Westfall, P. (2008). Simultaneous INference in General Paramteric Models. *Biometrical Journal, 50*(3), 346-363.

Ilvesaro, J., Tavi, P., & Tuukkanen, J. (2001). Connexin-mimetic peptide Gap 27 decreases osteoclastic activity. *BMC Musculoskeletal Discord, 2*(1), 10.

Jack, R. E., & Schyns, P. G. (2015, Jul 20). The Human Face as a Dynamic Tool for Social Communication. *Current Biology, 25*(14), R621-R634.

Jarvis, S. E., Lee, J. E., Jewlal, E., Barr, K., Kelly, G. M., Laird, D. W., & Willmore, K. E. (2020, Jul). Effects of reduced connexin43 function on skull development in

the Cx43I130T/+ mutant mouse that models oculdoentodigital dysplasia. *Bone, 136*, 115365.

Jewlal, E., Barr, K., Laird, D. W., & Willmore, K. E. (2021, Dec). Connexin 43 Contributes to Phenotypic Robustness of the Mouse Skull. *Developmental Dynamics, 250*(12), 1810-1827.

Jiang, J. X., Siller-Jackson, A. J., & Burra, S. (2007). Roles of gap junctions and hemichannels in bone cell functions and in signal transmission of mechanical stress. *Frontiers in Bioscience, 12*, 1450-1462.

Kalcheva, N., Qu, J., Sandeep, N., Garcia, L., Zhang, J., Wang, Z., . . . Fishman, G. I. (2007, Dec 18). Gap junction remodeling and cardiac arrhytmogenesis in a murine model of oculodentodigital dysplasia. *Proceedings of the National Academy of Sciences USA, 104*(51), 20512-6.

Klingenberg, C. P. (2003). *A developmental perspective on developmental instability: theory, models and mechanisms.* (M. Polak, Ed.) Oxford, UK: Oxford University Press.

Klingenberg, C. P. (2008). Morphological Integration and Developmental Modularity. *Annual Review of Ecology, Evolution, and Systematics, 39*, 115-132.

Klingenberg, C. P., & McIntyre, G. S. (1998). Geometric morphometrics of developmental instability: analyzing patterns of fluctuating asymmetry with Procrustes methods. *Evolution, 52*(5), 1363-1375.

Klingenberg, C. P., Barluenga, M., & Meyer, A. (2002). Shape Analysis of Symmetric Structures: Quantifying Variation Among Individuals and Asymmetry. *Evolution, 56*(10), 1909-1920.

Laird, D. (2014, Apr 17). Syndromic and non-syndromic disease-linked Cx43 mutations. *FEBS Letters, 588*(8), 1339-48.

Lazić, M. M., Carretero, M. A., Crnobrnia-Isailović, J., & Kaliontzopoulou, A. (2016). Canalization and developmental instability of hte fetal skull in a mouse model of maternal nutritional stress. *American Journal of Physical Anthropology, 43*(3), 368-379.

Leamy, L. J., & Klingenberg, C. P. (2005). The genetics and evolution of fluctuating asymmetry. *Annual Review of Ecology, Evolution, and Systematics, 36*, 1-21.

Lecanda, F., Warlow, P. M., Sheikh, S., Furlan, F., Steinberg, T. H., & Civitelli, R. (2000). Connexin43 Deficiency Causes Delayed Ossification, Craniofacial Abnormalities and Osteoblast Dysfunction. *The Journal of Cell Biology, 151*(4), 931-944.

Lima, F., Niger, C., Hebert, C., & Stains, J. P. (2009). Connexin43 Potentiates Osteoblast Responsiveness to Fibroblast Growth Factor 2 via a Protein Kinase C-Delta/Runx2-dependent Mechanism. *Molecular Biology of the Cell, 20*(11), 2697-2708.

Marieb, Mallatt, & Wilheld. (2013). *Human Anatomy 9th Ed.* Pearson/Cummins.

McLachlan, E., Plante, I., Shao, Q., Tong, D., Kidder, G. M., Bernier, S. M., & Laird, D. W. (2008). ODDD-linked Cx43 mutants reduce endogenous Cx43 expression and function in osteoblasts and inhibit late stage differentiation. *Journal of Bone Mineral Research, 23*(6), 928-38.

Meyer-Schwickerath, G., Gruterich, E., & Weyers, H. (1957). Klin Monatsblatter Augenheilkd Augenarztl Fortbild (The micropthalmos syndrome). *131*, 18-30.

Mitteroecker, P., & Bookstein, F. (2007, Oct). The Conceptual and Statistical Relationship between Modularity and Morphological Integration. *Systematic Biology, 56*(5), 818-836.

Mitteroecker, P., & Gunz, P. (2009, Mar 24). Advances in Geometric Morphometrics. *Evolutionary Biology, 36*, 235-247.

Moore, A. C., Wu, J., Jewlal, E., Barr, K., Laird , D. W., & Willmore, K. E. (2020). Effects of Reduced Connexin43 Function on Mandibular Morphology and Osteogenesis in Mutant Mouse Models of Oculodentodigital Dysplasia. *Calcified Tissue International, 107*(6), 611-624.

Niger, C., Buo, A. M., Hebert, C., Duggan, B. T., Williams , M. S., & Stains, J. P. (2012). ERK acts in parallel to PKC∂ to mediate the connexin43-dependent potentiation of Runx2 activity by FGF2 in MC3T3 osteoblasts. *American Journal of Physiology-Cell Physiology, 302*(7), C1035-C1044.

Olson, E. C., & Miller, R. (1958). *Morphological Integration.* Chicago: University of Chicago Press.

Olson, E. C., & Miller, R. L. (1958). *Morphological integration.* Chicago: University of Chicago Press.

Paznekas, W. A., Boyadieev, S. A., Shapiro, R. E., Daniels, O., Wollpik, B., Keegan, C. E., . . . Jabs, E. W. (2003). Connexin 43 (GJA1) Mutations Cause the Pleiotropic Phenotype of Oculodentodigital Dysplasia. *American Journal of Human Genetics, 72*(2), 408-418.

Paznekas, W. A., Karczeski, B., Vermeer, S., Lowry, R. B., Delatycki, M., Laurence, F., . . . Jabs, E. W. (2009). GJA1 mutations, variants ,and connexin 43 dysfunction as it relates to the oculodentodigital dysplasia phenotype. *Human Mutations, 30*(5), 724-33.

Percival, C. J., Marangoni, P., Tapaltsyan, V., Klein, O., & Hallgrímsson , B. (2017). The Interaction of Genetic background and Mutational Effects in Regulation of Mouse Craniofacial Shape. *G3 Genes|Genomes|Genetics, 7*(5), 1439-1450.

Plotkin, L. I., Speacht, T. L., & Donahue, H. J. (2015, Apr 1). Cx43 and Mechanotransduction in Bone. *Current Osteoporosis Reports, 13*(2), 67-72.

Pujadas , E., & Feinberg, A. P. (2012). Regulated noise in the epigenetic landscape of development and disease. *Cell, 148*(6), 1123-1131.

Ramler , D., Mitteroecker , P., Shama, L. N., Wegner, K. M., & Ahnelt, H. (2014, Mar). Nonlinear effects of temperature on body form and developmental canalization in the threespine stickleback. *Journal of Evolutionary Biology, 27*(3), 497-507.

Ramler, D., Mitteroecker, P., Shama, L. N., Wegner, K. M., & Ahnelt, H. (2014, Mar). Nonlinear effects of temperature on body form and developmental canalization in the threespine stickleback. *Journal of Evolutionary Biology, 27*(3), 497-507.

Ransjö, M., Sahli, J., & Lie, A. (2003). Expression of connexin 43 mRNA in microisolated murine osteoclasts and regulation of bone resorption in vitro by gap junction inhibitors. *Biochemical and Biophysical Research Communications, 303*(4), 1179-1185.

Rendel, J. M. (1959). Canalization of the Acute Phenotype of Drosophila. *International Journal of Organic Evolution, 13*(4), 425.

Rendel, J. M. (1967). *Canalisation and gene control.* Academic Press.

Riquelme, M. A., Cardenas, E. R., Xu, H., & Jiang, J. X. (2020). The Role of Connexin Channels in the Response of Mechanical Loading and Unloading of Bone. *International Journal of Molecular Sciences, 21*(3), 1146.

Rohlf, F. J., & Corti, M. (2000). Use of Two-Block Partial Least-Squares to Study Covariation in Shape. *Systematic Biology, 49*(4), 740-753.

Rutherford, S. L. (2000). From genotype to phenotype: buffering mechanisms and the storage of genetic information. *Bioessays, 22*, 1095-1105.

Rutherford, S. L. (2003). Between genotype and phenotype: protein chaperones and evolvability. *Nature Reviews Genetics, 4*(4), 263-274.

Rutherford, S. L., & Lindquist, S. (1998, Nov 26). Hsp90 as a capacitor for morphological evolution. *Nature, 396*(6709), 336-42.

Ryding, S., Klaassen, M., Tattersall, G. J., Gardner, J. L., & Symonds, M. R. (2021, Sep 7). Shape-shifting: changing animal morphologies as a response to climatic warming. *Trends in Ecology & Evolution*.

Sørensen, J. G., Kristensen, T. N., & Loeschcke, V. (2003). The evolutionary and ecological role of heat shock proteins. *Ecology Letters, 6*, 1025-1037.

Santagati, F., & Rijli, F. M. (2003, Oct). Carnial neural crest and the building of the vertebrate head. *Nature Reviews Neuroscience, 4*(10), 806-18.

Scharloo, W. (1991). Canalization: genetic and developmental aspects. *Annual Review of Ecological Systems, 22*, 65-93.

Scharloo, W. (1991). Canalization: Genetic and Developmental Aspects. *Annual Review of Ecology and Systematics, 22*(1), 65-93.

Stains, J. P., & Civitelli, R. (2005). Gap junctions in skeletal development and function. *Biochemica et Biophysica Acta- Biomembranes, 1719*(1-2), 69-81.

Stains, J. P., Watkins, M. P., Grimston, S. K., Hebert, C., & Civitelli, R. (2014, Jan 1). Molecular Mechanisms of Osteoblast/Osteocyte Regulation by Connexin43. *Calcified Tissue International, 94*(1), 55-67.

Steinacher, A., Bates, D. G., Akman, O. E., & Soyer, O. S. (2016). Nonlinear Dynamics in Gene Regulation Promote Robustness and Evolvability of Gene Expression Levels. *PLOS One, 11*(4), e0153295.

Stewart, M. K., Gong, X.-Q., Barr, K. J., Bai, D., Fishman, G. I., & Laird, D. W. (2013). The severity of mammary gland developmental defects is linked to the overall functional status of Cx43 as revealed by genetically modified mice. *Biochemical Journal, 449*(2), 401-413.

Taylor, A. F., Saunders , M. M., Shingle, D. L., Cimbala, J. M., Zhou, Z., & Donahue, H. J. (2007). Mechanically stimulated osteocytes regulate osteoblastic activity via

gap junctions. *American Journal of Physiology-Cell Physiology, 292*(1), C545-C552.

Van Valen, L. V. (1962). A study of fluctuating asymmetry. *Evolution, 16*(2), 125-142.

Varón-González, C., Pallares, L. F., Debat, V., & Navarro, N. (2019, Feb 12). Mouse Skull Mean Shape and Shape Robustness Rely on Different Genetic Architectures and Different Loci. *Frontiers in Genetics, 10*(64).

Vyas, B., Nandkishore, N., & Sambasivan, R. (2020). Vertebrate cranial mesoderm: developmental trajectory and evolutionary origin. *Cellular and Molecular Life Sciences, 77*, 1933-1945.

Waddington, C. H. (1942). Canalization of development and the inheritance of acquired characters. *Nature, 150*(3811), 563-565.

Waddington, C. H. (1953). The genetic assimilation of an acquired character. *Evolution, 7*, 118-26.

Waddington, C. H. (1957). *The Strategy of the Genes.* New York: MacMillan Publishing Company.

Wagner, G. P., & Altenberg, L. (1996). Perspective: Complex Adaptations and the Evolution of Evolvability. *Evolution, 50*(3), 967-976.

Watkins, M., Grimston, S. K., Norris, J. Y., Guillotin, B., Shaw, A., Beniash, E., & Civitelli, R. (2011). Osteoblast connexin43 modulates skeletal architecture by regulating both arms of bone remodeling. *Molecular Biology of the Cell, 22*(8), 1240-1251.

Wilkins, A. S. (2002). *The evolution of developmental pathways.* Sunderland, MA: Sinauer Associates.

Wilkins, J. F. (2005). Genomic imprinting and methylation: epigenetic canalization and conflict. *Trends Genet, 21*(6), 356-365.

Willmore, K. E., Klingenberg, C. P., & Hallgrímsson, B. (2005). The Relationship between Fluctuating Asymmetry and Environmental Variance in Rhesus Macaque Skulls. *Evolution, 59*(4), 898-909.

Willmore, K. E., Young, N. M., & Richtsmeier, J. T. (2007). Phenotypic Variability: Its Components, Measurement and Underlying Developmental Processes. *Evolutionary Biology, 34*(3-4), 99-120.

Young, N. M., Chong, H. J., Hu, D., Hallgrímsson, B., & Marcucio, R. S. (2010). Quantitative analyses link modulation of sonic hedgehog signaling to continuous variation in facial growth and shape. *Development, 137*(20), 3405-3409.

Zabinsky, R. A., Mason, G. A., Queitsch, C., & Jarosz, D. F. (2019). It's not magic -- Hsp90 and its effects on genetic and epigenetic variation. *Seminars in Cell and Developmental Biology, 88*, 21-35.

Zelditch, M. L., Swiderski, D. L., & Fink, W. L. (2004). *Geometric Morphometrics for Biologists: A Primer.* Academic Press.

5   Appendices
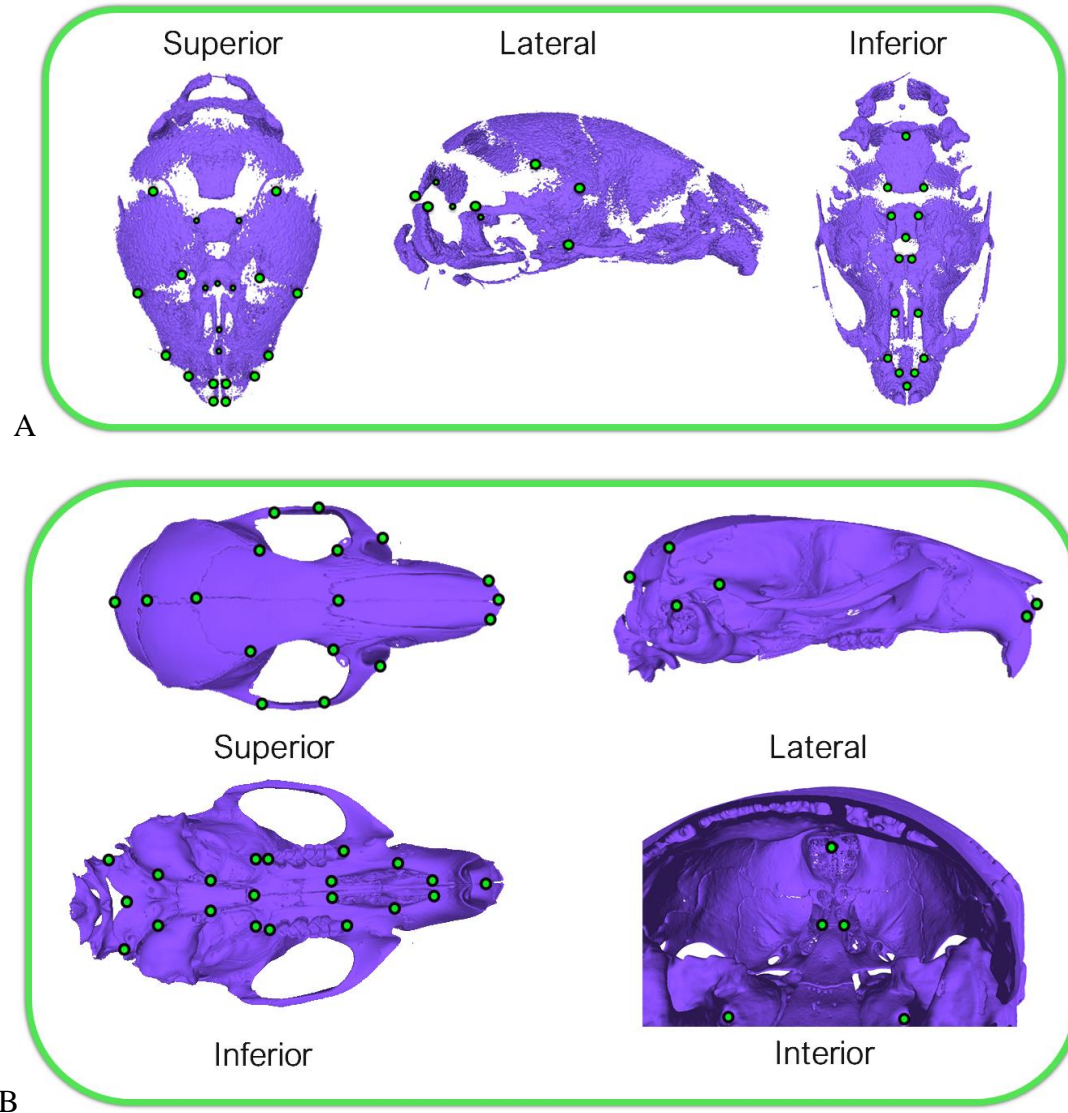
5.1   Landmarks

Figure 10 Landmarks

53 landmarks were used for each age point and are shown on mouse skull µCT scans as green circles. A. P0 Landmarks. B. Adult Landmarks

5.2   Approval of Animal Use Protocol

AUP Number: 2018-061
PI Name: Willmore, Katherine
AUP Title: Phenotypic and Biomechanical Effects of Altered Cell Proliferation and Differentiation in the Mouse Skull

Official Notification of ACC Approval: A modification to Animal Use Protocol **2018-061** has been approved.

Please at this time review your AUP with your research team to ensure full understanding by everyone listed within this AUP.

As per your declaration within this approved AUP, you are obligated to ensure that:

1. This Animal Use Protocol is in compliance with:
o Western's Senate MAPP 7.12 [PDF]; and
o Applicable Animal Care Committee policies and procedures.

2. Prior to initiating any study-related activities—as per institutional OH&S policies—all individuals listed within this AUP who will be using or potentially exposed to hazardous materials will have:

o Completed the appropriate institutional OH&S training; o Completed the appropriate facility-level training; and
o Reviewed related (M)SDS Sheets.

Submitted by: McInnis, Jennifer on behalf of the Animal Care Committee

Dr.Timothy Regnault,
Animal Care Committee Chair

Animal Care Commitee
The University of Western Ontario London, Ontario Canada N6A 5C1

ACC Website

5.3   Copyright Permission

License Number	5204410374705
License date	Dec 08, 2021
Licensed Content Publisher	John Wiley and Sons
Licensed Content Publication	Developmental Dynamics
Licensed Content Title	Connexin 43 contributes to phenotypic robustness of the mouse skull
Licensed Content Author	Elizabeth Jewlal, Kevin Barr, Dale W. Laird, et al
Licensed Content Date	Jun 24, 2021
Licensed Content Volume	250
Licensed Content Issue	12
Licensed Content Pages	18
Type of use	Dissertation/Thesis
Requestor type	Author of this Wiley article
Format	Print and electronic
Portion	Full article
Will you be translating?	No
Title	Connexin 43 contributes to phenotypic variability of the mouse skull
Institution name	Western University
Expected presentation date	Dec 2021
Order reference number	1066
Publisher Tax ID	EU826007151

Curriculum Vitae

Name: Elizabeth Jewlal

Post-secondary   University of Western Ontario
Education and   London, Ontario, Canada
Degrees: 2010-2016 B.A. (Hons)
Honours and
Awards: Ontario Graduate Scholarship (2019)
                    CMHR Trainee Program, Bone & Joint Institute (2017-present)
                    Western Graduate Research Scholarship (2017-present)
                    (B.A.) Don Wright Mustang Band Award (2015)
                    (B.A.) The Western Scholarship of Excellence (2010)

Related Work   Teaching Assistant
Experience   The University of Western Ontario (2017-2020)

                    Research Assistant
                    London Health Sciences Centre (2011-2016)

Publications:

Jewlal, E., Barr, K., Laird, D. W., & Willmore, K. E. (2021, Dec). Connexin 43 Contributes to Phenotypic Robustness of the Mouse Skull. *Developmental Dynamics, 250*(12), 1810-1827.

Moore, A. C., Wu, J., **Jewlal, E**., Barr, K., Laird , D. W., & Willmore, K. E. (2020). Effects of Reduced Connexin43 Function on Mandibular Morphology and Osteogenesis in Mutant Mouse Models of Oculodentodigital Dysplasia. *Calcified Tissue International, 107*(6), 611-624.

Jarvis, S. E., Lee, J. E., **Jewlal, E**., Barr, K., Kelly, G. M., Laird, D. W., & Willmore, K. E. (2020, Jul). Effects of reduced connexin43 function on skull development in the Cx43I130T/+ mutant mouse that models oculdoentodigital dysplasia. *Bone, 136*, 115365.

Abitbol, J. M., O'Donnell, B. L., Wakefield, C. B., **Jewlal, E**., Kelly, J. J., Barr, K., Willmore, K. E., Allman, B. L., Penuela, S. (2019, Mar). Double deletion of Panx1 and Panx3 affects skin and bone but not hearing. *Journal of Molecular Medicine*, 1-14.

Corkum, M. T., Shaddick, H., **Jewlal, E**., Patil, N., Leung , E., Sugimoto, A., . . . D'Souza, D. (2019, Jan). When Pap Testing Fails to Prevent Cervix Cancer: A Qualitative Study of the Experience of Screend Women Under 50 with Advanced Cervix Cancer in Canada. *Cureus Journal of Medicine, 11*(1), e3950.